

# Model Independent Determination of the Solar Neutrino Spectrum with and without MSW

Naoya Hata\* and Paul Langacker

*Department of Physics, University of Pennsylvania,  
Philadelphia, Pennsylvania 19104*

(September 20, 1994, UPR-0625T, hep-ph/9409372)

## Abstract

Besides the opportunity for discovering new neutrino physics, solar neutrino measurements provide a sensitive probe of the solar interior, and thus a rigorous test of solar model predictions. We present model independent determinations of the neutrino spectrum by using relevant flux components as free parameters subject only to the luminosity constraint. (1) Without the Mikheyev-Smirnov-Wolfenstein (MSW) effect, the best fit for the combined data is poor. Furthermore, the data indicate a severe suppression of the  ${}^7\text{Be}$  flux relative to the  ${}^8\text{B}$ , contradicting both standard and nonstandard solar models in general; the  $pp$  flux takes its maximum value allowed by the luminosity constraint. This pathology consistently appears even if we ignore any one of the three data. (2) In the presence of the two-flavor MSW effect, the current constraint on the initial  ${}^8\text{B}$  flux is weak, but consistent with the SSM and sufficient to exclude nonstandard models with small  ${}^8\text{B}$  fluxes. No meaningful constraint is obtained for the other fluxes. In the future, even allowing MSW, the  ${}^8\text{B}$  and  ${}^7\text{Be}$  fluxes can be determined at the  $\pm(15 - 20)\%$  level, making competing solar models distinguishable. We emphasize that the neutral current sensitivity for  ${}^7\text{Be}$  neutrinos in BOREXINO, HELLAZ, and HERON is essential for determining the initial fluxes. The constraints on the MSW parameters in the model independent analysis are also discussed.

Typeset using REVTeX

## I. INTRODUCTION

The solar neutrino deficit, confirmed by all existing experiments, challenges our understanding of the Sun as well as of neutrinos. The purpose of this paper is to consider the possibility of model independent determinations of the principle neutrino flux components from the solar neutrino data, both at present and in the future and with and without new neutrino properties. These fluxes can then be compared with the prediction of any solar model, standard or nonstandard. In fact, if the present experiments [1–7] are correct, purely astrophysical explanations for the flux deficit are highly unlikely:

- The standard solar models (SSMs) [8,9] are excluded by the data as summarized in Table I. The discrepancy cannot be reconciled by simply changing input parameters in the SSM calculations [10].
- The lower observed rate of Homestake relative to Kamiokande is incompatible with astrophysical solutions <sup>1</sup> in general. This is a much more serious difficulty than the simple deficit of observed neutrinos relative to the SSM expectations. <sup>2</sup> A model independent analysis [11] suggests a complete elimination of the <sup>7</sup>Be flux and, in addition, a larger depletion of the <sup>8</sup>B spectrum at lower energies and/or additional neutral current events from  $\nu_\mu$  or  $\nu_\tau$  in Kamiokande. The larger suppression of the <sup>7</sup>Be than the <sup>8</sup>B flux contradicts nonstandard solar models in general, including ad hoc ones. A distortion of the <sup>8</sup>B energy spectrum cannot be caused by astrophysical effects at the observable level [12].  $\nu_\mu$  and  $\nu_\tau$  can interact through the neutral currents in electron scattering in Kamiokande, and their existence in the solar flux signifies neutrino flavor

---

<sup>1</sup> By astrophysical solutions, we include those involving nuclear reaction cross sections in the Sun, but not the chlorine and gallium detector cross sections.

<sup>2</sup>In fact, the discrepancy in the relative rate is *aggravated* in models in which the <sup>8</sup>B flux is reduced (e.g., by lowering the core temperature or reducing the <sup>7</sup>Be( $p, \gamma$ )<sup>8</sup>B cross section) to explain the Kamiokande data.

oscillations.

- The problem of the larger suppression of the  ${}^7\text{Be}$  flux relative to  ${}^8\text{B}$  remains even if we ignore any one of the three data. In this sense, the data are consistent with each other. In particular, if we consider the Kamiokande and the gallium results only, the nonstandard solar models consistent with the Kamiokande result generally predict a gallium rate larger than 100 SNU, <sup>3</sup> inconsistent with the combined result of SAGE and GALLEX ( $77 \pm 9$  SNU).

With standard neutrino physics, the current situation forces us to consider a serious problem with two or more of the experiments *and* a drastic revision of the SSM calculation unless all of the experiments are wrong. The Mikheyev-Smirnov-Wolfenstein (MSW) mechanism [13], on the other hand, provides a complete description of the data and is also consistent with the SSM (see [14] and references therein). Because of the consistency with the experiments and the simplicity of the theory, we consider the two-flavor MSW solutions as the most attractive scenario among many proposed particle physics solutions.

For solar astronomy, whether new neutrino physics is present or not, the central issue is the determination of the solar neutrino spectrum. The theory of the Sun, which is the best measured main sequence star, is the keystone of our understanding of stellar structure and evolution. Solar neutrinos are a direct, sensitive probe of the solar core, and the neutrino flux measurements provide an opportunity for rigorous tests of solar models, standard or nonstandard.

For the SSM, the neutrino spectrum is a diagnostic of the underlying assumptions in the theory. The flux prediction depends on the input physics, such as the opacity calculation and the nuclear cross sections, whose uncertainties might be underestimated. In particular, the  $p({}^7\text{Be}, {}^8\text{B})\gamma$  cross section, which is directly proportional to the  ${}^8\text{B}$  flux, was recently measured using the Coulomb dissociation method in the RIKEN experiment [15]. Although

---

<sup>3</sup>SNU (solar neutrino unit) =  $1/10^{36}$  atoms /sec.

the measurement uncertainty is still large, the preliminary result suggests the cross section can be 25% lower than the current standard value [16]. The SSM also includes simplifications such as the omission of rotations, magnetic fields, and the gravitational settling of various elements. Those effects on the neutrino flux have never been quantified in the SSM uncertainties.

The nonstandard solar models, most of which are constructed to explain the solar neutrino deficit, assume nonstandard input parameters or nonstandard mechanisms. Examples are the low central temperature ( $T_C$ ), low opacity, low  $Z$ , large  $S_{11}$ , <sup>4</sup> large  $S_{33}$ , small  $S_{34}$ , small  $S_{17}$ , mixing, and weakly interacting massive particle (WIMP) models. The neutrino data should test the validity of such (often ad hoc) assumptions.

To determine the solar neutrino spectrum from the experiments, one needs to extract from the data the magnitude of the flux, component by component. The Kamiokande experiment measures the  $^8\text{B}$  flux exclusively. The radio-chemical detectors measure the flux components only as a weighted sum according to the energy dependence of the detector cross sections: the Homestake chlorine experiment is sensitive mainly to the  $^8\text{B}$  flux, but also to the  $^7\text{Be}$ , CNO, and  $pep$  fluxes; the gallium experiments measure all components, including the dominant  $pp$  flux. In the future, the Sudbury Neutrino Observatory (SNO) [17], Super-Kamiokande [18] and ICARUS [19] will measure the  $^8\text{B}$  flux with a high precision. BOREXINO [20] will be capable of measuring the  $^7\text{Be}$  line spectrum. HELLAZ [21], and HERON [22] will observe the  $^7\text{Be}$  flux and the main  $pp$  flux individually.

This solar neutrino spectroscopy can be complicated if new particle physics effects are present, since those effects are often energy dependent and therefore distort the energy spectrum. Uncertainties in the neutrino parameters contribute to uncertainties in the neutrino flux, and vice versa. In the presence of the MSW effect, for example, the determination of the initial (undistorted) flux components requires a knowledge of the neutrino parame-

---

<sup>4</sup>  $S_{11}$ ,  $S_{33}$ ,  $S_{34}$ , and  $S_{17}$  are the S factors proportional to the cross sections for  $p+p \rightarrow ^2\text{H}+e^++\nu_e$ ,  $^3\text{He}+^3\text{He} \rightarrow ^4\text{He}+2p$ ,  $^3\text{He}+^4\text{He} \rightarrow ^7\text{Be}+\gamma$ , and  $p+^7\text{Be} \rightarrow ^8\text{B}+\gamma$ , respectively.

ters and, in turn, the determination of the neutrino parameters depends on the initial flux magnitudes.

To extricate the neutrino flux components from the data and distinguish various competing solar models, it is best to consider a simple and general theoretical framework including all standard and nonstandard solar models. Such an analysis scheme should be viable with and without particle physics effects.

Variations of solar models have usually been considered in model dependent frameworks. Monte Carlo SSMs [23,24,10] were obtained from various input parameters normally distributed about their most probable values. Those solar models are, however, calculated within the SSM and do not address the possibility of nonstandard processes omitted in the modeling or the possibility of input parameters grossly different from the standard values. The low  $T_C$  model [25–27] parameterizes the neutrino fluxes by nonstandard core temperatures as power laws [23,24]. The description is more general than the Monte Carlo SSMs since it includes a large class of nonstandard solar models. Again, however, the  $T_C$  description is model dependent: there are nonstandard solar models that cannot be parametrized simply by nonstandard  $T_C$ , such as those with nonstandard  $S_{17}$  or  $S_{34}$  values.

In this paper, we consider a model independent description of solar models, characterized by the magnitude of each of the neutrino flux components. By setting up an analysis scheme as general as possible, we depart from particular theoretical constraints. We hope that the experiments will distinguish standard and nonstandard models and eventually identify the correct solar model. The purpose of this paper is to demonstrate that such a description is feasible and is a powerful tool in analyzing the solar neutrino data, especially once the high precision data from the next generation experiments are available.

Our model independent analysis originates in Ref. [11] (see also Ref. [28,27]). Here we elaborate the analysis and extend it to the case in which the two-flavor MSW effect is present. (Of course, the analysis can be generalized in the presence of any particle physics effect.) We consider magnitudes of the four prominent flux components,  $pp$ ,  ${}^7\text{Be}$ ,  ${}^8\text{B}$ , and CNO (the sum of  ${}^{13}\text{N}$  and  ${}^{15}\text{O}$ ), as free parameters in fitting data. In doing so, we make

minimal assumptions:

- The Sun is in a quasi-static state, and the solar luminosity is generated by the ordinary nuclear reactions of the  $pp$  and CNO chains. This imposes a relation among the fluxes:

$$\phi(pp) + \phi(pep) + 0.958 \phi(\text{Be}) + 0.955 \phi(\text{CNO}) = 6.57 \times 10^{10} \text{ cm}^{-2}\text{s}^{-1}, \quad (1)$$

where  $\phi(\text{CNO})$  is the sum of the  $^{13}\text{N}$  and  $^{15}\text{O}$  fluxes, which are varied with the same scale factor.

- Astrophysical mechanisms do not distort the shape of the energy spectrum of the individual flux component at the observable level. It was shown that possible distortions of the spectrum due to such astrophysical effects as gravitational red-shifts and thermal fluctuations are completely negligible [12]. On the other hand, particle physics effects such as the MSW mechanism are in general energy dependent and lead to significant spectral distortions.
- The detector cross section calculations [23,24,29] are correct.
- The minor fluxes ( $pep$ <sup>5</sup>,  $^{17}\text{F}$ , and  $hep$ <sup>6</sup>) are set to the SSM values.

The simultaneous (global) analysis of all data is essential in obtaining constraints on fluxes. No one experiment provides enough information to determine the entire neutrino spectrum; only by combining various experiments with different energy thresholds is it possible to determine each flux component and test solar model predictions. For example, if there are no new particle physics effects, then by combining the  $^8\text{B}$  flux measured in

---

<sup>5</sup> The  $pep$  neutrinos are from the reaction  $p + e^- + p \rightarrow ^2\text{H} + \nu_e$ . The  $pep$  flux is the largest among the three minor fluxes. It is strongly correlated with the  $pp$  flux in many of the nonstandard solar models [30] and does not vary significantly from model to model. Of course, one can also use the  $pep$  flux as a free parameter.

<sup>6</sup>The  $hep$  neutrinos are from the reaction  $^3\text{He} + p \rightarrow ^4\text{He} + e^+ + \nu_e$ .

Kamiokande with the Homestake and gallium experiments, one can deduce an absence of the  ${}^7\text{Be}$  flux and a detection of the  $pp$  flux. Allowing for MSW or other particle physics effects, a global analysis is even more essential because one must simultaneously determine the initial fluxes and the MSW-induced flux reduction and spectral distortions.

In constraining the fluxes and testing solar models, a consistent joint analysis is important. Taking overlaps of parameter space allowed by different experiments does not yield a correct estimation of uncertainties [14]; one needs to carry out proper joint  $\chi^2$  analyses, which are essentially identical to the maximum likelihood method in gaussian cases. Since we are testing theoretical models statistically, the experimental and theoretical uncertainties have to be incorporated; a proper treatment of the correlations among uncertainties is also important [14].

When the MSW effect is present, it is best to incorporate available energy spectrum and day-night asymmetry data to obtain additional constraints on the neutrino parameters and therefore on the fluxes. Those constraints from future high-counting experiments would be especially useful. In this paper, however, we do not incorporate the existing energy spectrum and day-night data from Kamiokande [3]; their uncertainties are large and do not significantly change the results obtained from the averaged data. <sup>7</sup>

The rest of the paper is organized as the following. In Section II, the constraints on the fluxes without introducing particle physics effects are obtained. The joint fit of the combined the Homestake, Kamiokande, SAGE, and GALLEX data yields a poor  $\chi^2$  value. The best fit is, in fact, obtained for a negative  ${}^7\text{Be}$  flux, suggesting a serious problem with the experiments *or* the existence of new particle physics effects: a distortion of the  ${}^8\text{B}$  spectrum and/or neutral current contributions from  $\nu_\mu$  or  $\nu_\tau$  in Kamiokande. Even if we

---

<sup>7</sup> Also, Kamiokande has only presented the spectrum and angular (direction of the Sun with respect to the nadir) distributions separately. Since they are based on the same data, the two distributions are correlated and cannot be used simultaneously. It is recommended that in the future the data be presented in bins of definite energy *and* angle.

accept this poor fit assuming standard neutrinos, the constraint on the fluxes contradicts nonstandard solar models in general. The constraints on the fluxes will be displayed in the  ${}^7\text{Be}$ - ${}^8\text{B}$ ,  $pp$ - ${}^7\text{Be}$ , and  $pp$ - ${}^8\text{B}$  planes. (For simplicity, we refer to neutrino fluxes in units of the reference fluxes listed in Table II unless otherwise mentioned. Those fluxes correspond to the Bahcall-Pinsonneault fluxes with the helium diffusion effect [8]). The results when one of the three experiments are omitted will be also given. By ignoring one experiment, the uncertainties in the flux constraints become larger, but the constraints are consistent with those obtained from all data, and again contradict astrophysical/nuclear solutions.

In Section II, we also discuss possible constraints on the fluxes from the next generation experiments. In fact, if no new particle effects are present, SNO and Super-Kamiokande will determine the initial  ${}^8\text{B}$  flux with a high precision, and BOREXINO, HELLAZ, and HERON will measure the initial  ${}^7\text{Be}$  flux exclusively. The flux constraints from hypothetical results from these experiments with various central values and various measurement uncertainties will be examined.

In Section III, we consider the constraints on the fluxes when the two-flavor MSW effect for transitions  $\nu_e \rightarrow \nu_\mu$  or  $\nu_e \rightarrow \nu_\tau$  is present. Our analysis scheme can in principle be applied to other particle physics scenarios, such as three-flavor MSW, transitions into sterile neutrinos, vacuum oscillations, a large neutrino magnetic moment, neutrino decays, flavor changing neutral currents, violation of the equivalence principle, etc. We consider the two-flavor MSW solution because of its simplicity and viability. It is likely that if two-flavor MSW is indeed occurring, there will be enough complementary information [e.g., from spectral distortions, day-night asymmetries, and SNO neutral current (NC) measurements] to establish it as the most likely candidate even allowing nonstandard solar models [14]. Of course one could never rigorously exclude the possibility of more complicated scenarios, such as the simultaneous importance of transitions into  $\nu_\mu$  (or  $\nu_\tau$ ) and sterile neutrinos, which would interfere with the model independent flux determinations. For this, one must invoke Occam's razor.



Once the MSW parameters are introduced as additional free parameters in the joint fit, constraining the fluxes from the data is not trivial. The MSW effect can distort the energy spectrum depending on the parameters, and can change the contribution from different flux components. With the existing data, we can constrain the  $^8\text{B}$  flux only roughly. Even though the chlorine and gallium experiments have a sensitivity to the  $^7\text{Be}$  flux, the survival probability of the flux can be zero for the MSW small-angle (nonadiabatic) solution, and no meaningful constraint is obtained for the  $^7\text{Be}$  flux. To constrain the fluxes and the MSW parameters simultaneously, we need results from the future experiments, especially the neutral current measurement in SNO and the  $^7\text{Be}$  neutrino measurement in BOREXINO, HELLAZ, or HERON. The neutrino-electron scattering mode in these  $^7\text{Be}$  measurements has a sensitivity to the neutral current interactions with  $\nu_\mu$  and  $\nu_\tau$ , whose cross sections are 21% of  $\nu_e$ 's at this energy. We will present the possible constraints assuming various outcomes from those experiments, and show that such a model independent analysis can determine the solar neutrino spectrum with an accuracy sufficient to test solar model predictions. We note that our choice of the hypothetical results from the SNO NC and BOREXINO experiments are minimal; additional information from the SNO charged current (CC) rate, the Super-Kamiokande rate, and the spectral and day-night asymmetry measurements in SNO and Super-Kamiokande should make the constraints even better.

## II. FLUX CONSTRAINTS ASSUMING STANDARD NEUTRINOS

### A. Present

We consider the constraints on the neutrino fluxes from the updated solar neutrino data listed in Table I. The main results are displayed in the  $^7\text{Be}$ – $^8\text{B}$  plane (although some of the results are also shown in the  $pp$ – $^7\text{Be}$  and  $pp$ – $^8\text{B}$  planes). When the data are fit, the  $pp$  and CNO fluxes are varied freely for each  $\phi(\text{Be})$  and  $\phi(\text{B})$ , subject only to the luminosity constraint. This representation in the  $^7\text{Be}$ – $^8\text{B}$  plane is effective since it can display every possible solar model, standard or nonstandard, that satisfies our minimal assumptions. Since

predictions for those fluxes vary substantially from model to model, the  ${}^7\text{Be}$ - ${}^8\text{B}$  plane also provides a useful diagnostic for experimentally distinguishing competing solar models.

When the Kamiokande, Homestake, and the combined gallium experiments of SAGE and GALLEX are fit separately, the constraints on the  ${}^7\text{Be}$  and  ${}^8\text{B}$  fluxes are shown in Fig. 1. The fits include the uncertainties in the radio-chemical detector cross sections and in the minor fluxes, which are set to the SSM values. The Kamiokande result constrains the  ${}^8\text{B}$  flux; the Homestake result constrains the  ${}^7\text{Be}$ ,  ${}^8\text{B}$ , and CNO fluxes; the gallium results constrain all fluxes including the  $pp$ .

When all data are fit simultaneously, the allowed fluxes are severely constrained, as shown in Fig. 2. The best fit for physical (i.e., non-negative) fluxes are obtained for zero  ${}^7\text{Be}$  and CNO fluxes, and the  ${}^8\text{B}$  flux is about 40% of the SSM prediction; the absence of the  ${}^7\text{Be}$  and CNO fluxes forces the  $pp$  flux to be the maximum value (1.095 SSM) allowed by the luminosity constraint (Eq. 1). These constraints at  $1\sigma$  uncertainties are summarized in Table III; they are also listed as absolute fluxes in Table IV. This model independent result displays serious problems for any purely astrophysical explanation for the solar neutrino deficit [11]:

- The best fit is poor; the  $\chi^2$  minimum is in fact obtained for the unphysical value  $\phi(\text{Be})/\phi(\text{Be})_{\text{SSM}} = -0.5$ . Imposing positivity of the flux,  $\chi^2_{\text{min}} = 3.3/1$  d.f.,<sup>8</sup> which is excluded at 93% confidence level (C.L.) That is, any possible solar model explanation consistent with our minimal assumptions is excluded at least at the 93% C.L.
- Even if one accepts this poor fit, the allowed fluxes are difficult to explain. Since  ${}^8\text{B}$  is produced through the reaction  $p + {}^7\text{Be} \rightarrow {}^8\text{B} + \gamma$ , any reduction in  ${}^7\text{Be}$  causes at least an equal reduction in  ${}^8\text{B}$ . Therefore, unless there is some independent mechanism

---

<sup>8</sup>The fit is in fact for 0 d.f. [3 data - (4 parameters - 1 constraint)]. For  $\chi^2$  values other than zero, there is no standard statistical interpretation exists other than to conclude that this model is excluded. To quantify the confidence level, we allow 1 d.f. by considering that the  ${}^7\text{Be}$  flux is fixed to zero.

to suppress only the  ${}^7\text{Be}$  flux <sup>9</sup> or the uncertainty in the  ${}^7\text{Be}$  electron capture rate is grossly underestimated, the  ${}^8\text{B}$  flux is expected to be reduced more than the  ${}^7\text{Be}$  flux, contrary to the data.

- Finally, various standard and nonstandard models are also displayed in Fig. 2: the Bahcall-Pinsonneault SSM including the helium diffusion effect [8], the Bahcall-Ulrich 1000 Monte Carlo SSMs [23], Turck-Chièze–Lopes SSM [9], the low Z model [23,24], the low opacity models with the opacity reduced by 10 and 20% [31], the WIMP model [32], the large  $S_{11}$  models [33], the small  $S_{34}$  model [9], the large  $S_{33}$  model [9], the mixing models [34], the Dar-Shaviv SSM [35], and the high Y model [23,24]. Also shown are models parametrized by a lower  $T_C$  (which approximately incorporates many of the explicit models) and a lower  $S_{17}$ . As seen in Fig. 2, none of those solar model predictions are even close to the observations.

We also note that a lower  $S_{17}$  value, suggested by the RIKEN experiment [15], aggravates the problem with astrophysical/nuclear solutions, contrary to the general notion. A lower  $S_{17}$  value can make the theory prediction for the  ${}^8\text{B}$  flux smaller and closer to the Kamiokande result, which leaves little room to introduce other astrophysical/nuclear effects (e.g., a lower  $T_C$ ) to reduce the  ${}^7\text{Be}$  flux, failing to explain either the Homestake or the gallium results.

This complete phenomenological failure of astrophysical solutions suggests nonstandard particle physics effect such as the MSW effect, or serious problems with the experiments [11].

Even if only the Kamiokande and gallium results are considered, there is still essentially no viable theoretical explanation. Although the best fit somewhat improves ( $\chi^2/0 \text{ d.f.} = 1.2$ ), the obtained fluxes displayed in Fig. 3 are consistent with a complete depletion of the  ${}^7\text{Be}$  flux, while the  ${}^8\text{B}$  flux is about half of the SSM prediction (Table III and IV). This is

---

<sup>9</sup> For example, both  $\phi(\text{Be})$  and  $\phi(\text{B})$  could be suppressed by a low  $T_C$ , and  $\phi(\text{B})$  could then be enhanced by a *larger*  $S_{17}$ . However, for any realistic  $S_{17}$ , this enhancement would be negligible.

again in severe contradiction with nonstandard solar models in general. The nonstandard solar models that are significantly inside the 99% C.L. contour in Fig. 3(a) are the small  $S_{34}$  model, the large  $S_{33}$  model, and ad hoc mixing models that involve a core with 0.4 and 0.8 solar masses that is mixed continuously. These models also predict non-zero CNO fluxes, while the C.L. contours in Fig. 3 corresponds to zero CNO flux. The non-zero CNO contribution further aggravates the disagreement. When the CNO flux is fixed to the SSM value, the constraint for the combined Kamiokande and gallium results is displayed in Fig. 4.

The discrepancy between solar model solutions and the combined Kamiokande and gallium result can be described in another way. Nonstandard models yield a wide variety of fluxes, and therefore a large range for their gallium predictions: from the 78 SNU of the luminosity limit<sup>10</sup> to 303 SNU of the maximum rate model [8]. However, the  $^8\text{B}$  flux, which has the largest uncertainty among the major fluxes, has been constrained by Kamiokande, and this in turn constrains the gallium predictions of nonstandard models. Such a constraint was considered in the SSM framework with the Monte Carlo method [10], but here we allow nonstandard models as well. Displayed in Fig. 5 along with the gallium data are the gallium predictions of various SSMs and also of nonstandard solar models that are consistent with or close to the  $^8\text{B}$  flux observed in Kamiokande: the model with  $S_{17}$  normalized to the Kamiokande result, the low  $T_C$  model with a reduction of 4%, the model with a *larger*  $S_{17}$  (30%) and a lower  $T_C$  (5%), the low  $S_{34}$  (50%) model, the Dar-Shaviv SSM [35], the low opacity model [31], the large  $S_{11}$  models that predict  $\phi(\text{B})/\phi(\text{B})_{\text{SSM}} = 0.39$  [9] and 0.57 [33], and mixing models [34]. The uncertainties include the  $^8\text{B}$  uncertainty due to the Kamiokande uncertainty (14%), but the dominant contribution is from the gallium cross section uncertainty. From this list, we obtain

$$\text{Gallium rate consistent with Kamiokande } \gtrsim 100 \text{ SNU}, \quad (2)$$

---

<sup>10</sup> This corresponds to zero  $^7\text{Be}$ , CNO,  $pep$ , and  $^8\text{B}$  fluxes and the  $pp$  flux with the maximum value allowed by the luminosity constraint (Eq. 1).

while the combined gallium rate of SAGE and GALLEX is  $77 \pm 9$  SNU.

The lower limit of 100 SNU can be roughly understood as followings. The nonstandard solar models considered here all predict smaller reductions of the  ${}^7\text{Be}$  than the  ${}^8\text{B}$  flux, and this, combined with the Kamiokande result, gives the lower limit on the  ${}^7\text{Be}$  flux to be about half of the SSM value, contributing at least 18.3 SNU to the gallium rate. The  $pp$  and  $pep$  fluxes do not depend significantly on solar models; the luminosity constraint and a decrease in the  ${}^7\text{Be}$  flux result in an increase in the  $pp$  flux by 5% (3.7 SNU). Adding these ( $pp$ ,  $pep$ ,  ${}^7\text{Be}$ , and  ${}^8\text{B}$ ) gives a total of 102.9 SNU, with uncertainties in the treatment of the CNO fluxes, the gallium detector cross section, and the  ${}^8\text{B}$  measurement in Kamiokande.

This discrepancy is extremely important because it is independent of the Homestake result, but displays exactly the same symptom as in the Kamiokande-Homestake comparison: the absence of the  ${}^7\text{Be}$  flux, for which astrophysics offers no explanation. Furthermore, experimental developments in the near future will significantly influence the situation. The calibration of the gallium detectors with chromium sources will help understand the systematic uncertainty and the detector cross section, reducing the uncertainty. It is also important to continue the gallium experiments to the statistics limit to establish consistency or inconsistency with the 100 SNU benchmark. Theoretically, those models which predict 100 SNU can be compared with helioseismology data. In fact, some of the nonstandard models (the low  $T_C$  model [37], the large  $S_{11}$  model [9], the mixing model [36], and the low  $Y$  model [37]) are in conflict with the sound speed profile inferred from helioseismology observations and therefore excluded. Further detailed testing of those nonstandard solar models with helioseismology data would be welcome.

The flux constraints when the gallium and Kamiokande results are separately ignored are shown in Figs. 6 and 7. The flux constraints from various combinations of the existing data are summarized in Table III and IV. We note that any combination of two experiments are consistent with the complete absence of the  ${}^7\text{Be}$  and CNO fluxes, the  ${}^8\text{B}$  flux of about 40% of the SSM, and the maximum  $pp$  flux, contradicting astrophysical solutions in general. That is, we have to ignore two of the three data to find a reasonable astrophysical explanation of

the solar neutrino problem.

## B. Future

Since the current results are almost limited by systematic uncertainties, the present status described in the previous section is unlikely to change with the existing experiments unless there is a drastic revision in the data analyses. We expect, on the other hand, that our understanding of solar neutrinos will greatly improve once the results from the new generation of high-statistic experiments are available. SNO [17] and Super-Kamiokande [18] will start in 1996, measuring the  $^8\text{B}$  flux with high precision. The neutral current (NC) measurement in SNO and the measurements of the energy spectrum and time dependence in the two experiments will either confirm or rule out the neutrino oscillation hypothesis. BOREXINO [20] will operate later in the decade and measure the  $^7\text{Be}$  line spectrum separately. HELLAZ [21] and HERON [22] can measure the  $pp$  and  $^7\text{Be}$  neutrinos separately.

Assuming that neutrino physics effects are absent, we should be able to calibrate solar models with precision measurements of the  $^7\text{Be}$  and  $^8\text{B}$  fluxes, independent of the existing experiments. The relevant flux parameter space with various standard and nonstandard solar models is displayed in Fig. 8(a). The determination of the  $^7\text{Be}$  and  $^8\text{B}$  fluxes at better than the 20% level should distinguish between competing solar models. It is also important to compare the future results to the present constraints for a consistency check among the data.

For experiments sensitive to the  $pp$  flux, such as the gallium experiments, HELLAZ, and HERON, the relevant flux parameter space will be in Fig. 8(b) and (c). The  $pp$  flux is, however, strongly constrained by the solar luminosity, and, to further distinguish the competing solar models, measurement uncertainties as small as a few % will be required.

To study the sensitivity for determining the fluxes and distinguishing solar models, we have carried out a joint analysis assuming various possible outcomes from the new generation experiments. The constraint on the fluxes is shown in Fig. 9(a) when SNO or

Super-Kamiokande data are assumed to be  $0.50 \pm 0.05$  SSM. The allowed parameter space is for 90% C.L. The constraint on the  ${}^7\text{Be}$  flux from BOREXINO <sup>11</sup> data ( $1.0 \pm 0.1$  SSM) is displayed in Fig. 9(b). Displayed in Fig. 10(a) are the constraints on both fluxes when the  ${}^7\text{Be}$  flux is measured in BOREXINO at the SSM value with an experimental uncertainty of 10%; various values (0.3, 0.5, 0.7, and 1.0 SSM) for the  ${}^8\text{B}$  flux measurement are assumed with a 10% experimental uncertainty. Fig. 10(b) is the same except that various  ${}^7\text{Be}$  values are assumed for a fixed central value of the  ${}^8\text{B}$  flux ( $0.50 \pm 0.05$  SSM).

The constraints are shown in Fig. 11 when different experimental uncertainties are used for the  ${}^8\text{B}$  flux measurements and for BOREXINO. With measurement uncertainties at the 10% level in SNO, Super-Kamiokande, and BOREXINO, the  ${}^7\text{Be}$  and  ${}^8\text{B}$  fluxes are determined accurately enough that the observations can distinguish between standard and nonstandard solar models and perhaps even constrain the SSM parameters. The constraints from the future data should be compared with the current constraint (Fig. 2) for a consistency check.

### III. FLUX CONSTRAINTS ASSUMING MSW

#### A. Present

Once the MSW effect is introduced in the analysis, the calibration of the neutrino fluxes becomes more complicated. One must constrain the initial fluxes and the MSW parameters simultaneously, while the neutrino spectrum can be distorted depending on the MSW parameters. We consider the simplest scenario, the two-flavor MSW effect. With the three existing data points and using  $\Delta m^2$ ,  $\sin^2 2\theta$ , and  $\phi(\text{B})$  as completely free parameters, one obtains

$$\phi(\text{B})/\phi(\text{B})_{\text{SSM}} = 1.15 \pm 0.53 (1\sigma), \quad (3)$$

---

<sup>11</sup>The same analysis applies for the HELLAZ and HERON experiments.

while the other fluxes are fixed to the SSM values. Although the constraint is weak, it is consistent with the SSM predictions and already excludes (in the MSW context) some of the nonstandard models with a smaller  ${}^8\text{B}$  flux. Since half of the SSM  ${}^8\text{B}$  flux is seen in Kamiokande and since the MSW effect only reduces observed rates, the  ${}^8\text{B}$  flux cannot be too small. Taking into account the Homestake and gallium data and also the neutral current contribution in Kamiokande, the 90% lower and upper limit is 0.47 and 2.07 of SSM, respectively. The constraint at 90% C.L. is displayed in Fig. 12. The  $\chi^2$  distribution and the corresponding constraints on the MSW parameters are shown in Fig. 13.

If the  ${}^7\text{Be}$  flux is introduced as an additional free parameter, no realistic constraint is obtained, even though the chlorine and gallium experiments have sensitivity to the flux. This is because the MSW survival probability for the  ${}^7\text{Be}$  flux can be zero, allowing essentially any amplitude for the initial flux. In principle, the  ${}^7\text{Be}$  flux has an upper limit due to the luminosity constraint, but the constraint is weak and irrelevant. We have repeated the fit by assuming smaller uncertainties for all experiments and by incorporating the Kamiokande spectral and day-night data [3], but no constraint was obtained for the  ${}^7\text{Be}$  flux. If MSW is operative, one needs a neutral current sensitivity for the flux (as in BOREXINO, HELLAZ, and HERON) to extract the  ${}^7\text{Be}$  amplitude, which we will discuss in the next section.

The core temperature, although model dependent, can be determined from the existing data using the power law for the  ${}^7\text{Be}$  and  ${}^8\text{B}$  fluxes. The power law obtained from a Monte Carlo estimation is

$$\phi(\text{Be}) \sim T_C^8 \quad \text{and} \quad \phi(\text{B}) \sim T_C^{18}, \quad (4)$$

and the  $T_C$  dependence of the  $pp$  flux is obtained from the above relation and the luminosity constraint (Eq. 1), assuming the exponents of the  $pep$  and CNO fluxes as 2.8 and 22, respectively [14]. The flux uncertainties from the nuclear reaction cross sections are included for  $S_{17}$  and  $S_{34}$  as described in [14]. The detector cross section uncertainties for chlorine and gallium are also included. As a result of a three parameter fit (two MSW parameters and  $T_C$ ) [26,14], we obtain



$$T_C = 1.00 \pm 0.03 (1\sigma) \tag{5}$$

in units of the SSM prediction ( $T_C = 1 = 15.57 \times 10^6$  K). The result is consistent with the SSM ( $T_C = 1 \pm 0.006$ ). That is, allowing the MSW effect, the present data determine  $T_C$  to within 3% and are consistent with the SSM predictions. We note that without the MSW effect no temperature could describe the data simultaneously [25,26,38]. The  $\chi^2$  distribution and the constraints on the MSW parameters are shown in Fig. 14.

### B. Future

In the next decade or so, the new generation of solar neutrino experiments will start and provide high-statistics data. Those experiments will measure the fluxes precisely and will allow a separation of the  $^8\text{B}$ ,  $^7\text{Be}$ , and  $pp$  fluxes. Then, to determine the initial neutrino spectrum in the presence of nonstandard particle physics effects, what needs to be measured, and with what accuracy?

We answer these questions quantitatively in the model independent framework, assuming two-flavor MSW oscillations, since it is the simplest solution of the solar neutrino problem and most successful in describing the existing data.<sup>12</sup> We assume that the measurement of the charged to neutral current ratio in SNO will establish neutrino oscillations. We also assume that the measurement of the energy spectrum distortions and the day-night effect in SNO and Super-Kamiokande will distinguish the three separate MSW parameter branches from each other [14] and from vacuum oscillations [39]. The adiabatic and nonadiabatic regions will show  $^8\text{B}$  spectrum depletion at higher and lower energies, respectively, which will be observable in SNO and Super-Kamiokande [14]. Most of the large-angle region shows the Earth effect, which will be measurable as day-night asymmetries or diurnal signal variations in SNO, Super-Kamiokande, and BOREXINO [14,40]. Since the spectrum and time-

---

<sup>12</sup> Similar analyses should be applicable to other particle physics effects if they do not involve too many new parameters.

variation information constrain the MSW parameters independent of the flux uncertainties, it would be best to incorporate those data directly in the analysis once the actual data are available. At present, however, we do not attempt to consider such constraints. We only consider the averaged SNO NC and BOREXINO rate (and the averaged Super-Kamiokande rate for some cases) as the minimal hypothetical data from the future experiments. Even so, one should be able to determine all of the parameters reasonably well.

In the MSW calculations, we employ the electron density profile function and the neutrino production profile functions of the Bahcall-Pinsonneault SSM. These functions are solar model dependent and should, in principle, be an additional source of uncertainties in constraining the fluxes and the MSW parameters. We have previously investigated those uncertainties by using three different SSMs and also by changing the peak location of the production profiles and the electron density scale height by 10% each [14]. The effect on the obtained MSW parameters was negligible in the combined fit.

In Figures 15–19, we consider the flux constraints for various possible outcomes of the SNO NC, BOREXINO, and Super-Kamiokande experiments that are consistent with the assumption that the MSW parameters are in the nonadiabatic (diagonal) branch. We include the current results of the Homestake, (time-averaged) Kamiokande, and the combined gallium experiments, incorporating the detector cross section uncertainties in the radiochemical experiments. However, omitting either the Homestake or gallium results does not change the result significantly, which will allow us to check consistency among data in the future. The constraints are obtained by fits to five free parameters [ $\phi(pp)$ ,  $\phi(\text{Be})$ ,  $\phi(\text{B})$ ,  $\Delta m^2$ , and  $\sin^2 2\theta$ ] imposing the luminosity constraint. The CNO and the minor fluxes are fixed to the SSM values. As shown later, using the CNO flux as an additional free parameter does not change our results significantly.

Fig. 15(a) displays the constraints on the  ${}^7\text{Be}$  and  ${}^8\text{B}$  fluxes at 90% C.L. when the result of the SNO NC measurement is assumed to be the SSM value. The current data from Homestake, Kamiokande, SAGE, and GALLEX are also included. The measurement uncertainties are taken as 10% of the signal. The SNO NC rate is unaffected by flavor oscillations, and

yields a direct measurement of the  $^8\text{B}$  flux.<sup>13</sup> The  $^7\text{Be}$  flux is not constrained even though the chlorine and gallium detectors have sensitivity, because the  $\nu_e$  survival probability for this energy range can be zero, and therefore the initial  $^7\text{Be}$  flux can take essentially any value.

When the  $^7\text{Be}$  measurement from BOREXINO<sup>14</sup> is assumed to be  $0.24 \pm 0.024$  of the SSM value, the allowed region is shown in Fig. 15(b); the existing data are also included, but not the SNO result. Interestingly, both the  $^7\text{Be}$  and  $^8\text{B}$  fluxes are constrained in this case. The crucial factor is that, in electron scattering experiments, there is a contribution of the neutral current events from the  $\nu_\mu$  or  $\nu_\tau$  into which  $\nu_e$  oscillates. For the  $^7\text{Be}$  line spectrum at 0.862 MeV, the  $\nu_\mu - e$  (or  $\nu_\tau - e$ ) cross section is 21% of the  $\nu_e - e$ . Therefore there should be a signal of at least 21% of the initial flux even if the  $\nu_e$  survival probability is zero. The BOREXINO result, combined with the existing data, gives a stringent constraint on both the original  $^7\text{Be}$  flux and the MSW parameters, and those, in turn, constrain the  $^8\text{B}$  flux when combined with the Kamiokande result.

The results when both the SNO NC and BOREXINO data are assumed for various different central values are shown in Fig. 16. The MSW regions for the same or similar SNO NC and BOREXINO results are displayed in Fig. 17. Considering that the constraints are independent of solar models, the allowed regions are determined surprisingly well. We also note that the information of the spectral distortion and of the day-night asymmetry, which is ignored here, will distinguish the adiabatic, nonadiabatic, and large-angle regions, and

---

<sup>13</sup> The charged current (CC) measurement in SNO, combined with the NC result, will determine the survival probability of the  $^8\text{B}$  flux. Once neutrino oscillations are established, however, this information will not significantly improve the Kamiokande result included here. The effect of the CC measurement uncertainties are similar to the effect of the Super-Kamiokande measurement uncertainties discussed below.

<sup>14</sup> Our results apply for other  $^7\text{Be}$  measurements with electron scattering, such as in HELLAZ and HERON.

therefore further constrain the MSW parameters.

The effect on the flux constraints for various measurement uncertainties for SNO NC and BOREXINO are shown in Fig. 18. Shown in Fig. 19 is the constraint when the result from Super-Kamiokande is included for different measurement uncertainties.

The effect of using the CNO flux as an additional free parameter is displayed in Fig. 20; the result is essentially unchanged.

The analysis has been repeated assuming measurements consistent with the MSW large-angle branch. The constraints from each SNO NC and BOREXINO measurement and the combined SNO NC and BOREXINO are displayed in Fig. 21 and Fig. 22. The other results are essentially the same as for the nonadiabatic branch.

From the analysis above, we conclude that, if the SNO NC and BOREXINO uncertainties are at the 10% level relative to signal, the  ${}^7\text{Be}$  and  ${}^8\text{B}$  fluxes should be constrained at the  $\pm 20\%$  and  $\pm 15\%$  level, respectively. This will clearly distinguish the standard and nonstandard solar models and perhaps even constrain the SSM parameters. The neutral current reaction for the  ${}^7\text{Be}$  measurement ensures a non-zero signal (assuming flavor oscillations), which is especially important for obtaining stringent constraints on the neutrino fluxes and for distinguishing between competing solar models.

Although model dependent, we have also carried out a simultaneous fit of  $T_C$  and  $S_{17}$  with hypothetical outcome from SNO NC and BOREXINO. The current data are also included. The constraint on  $T_C$  and  $S_{17}$  is shown in Fig. 23.  $T_C$  and  $S_{17}$  will be simultaneously determined at the  $\pm 4\%$  and  $\pm 20\%$  level (90% C.L.)

#### IV. CONCLUSION

We have demonstrated that a model independent analysis using the four relevant fluxes ( $pp$ ,  ${}^7\text{Be}$ ,  ${}^8\text{B}$ , and CNO) as free parameters subject to the luminosity constraint is a feasible scheme for neutrino spectroscopy, and therefore for testing solar models. The analysis is viable with both standard and nonstandard neutrinos.

Assuming standard neutrinos, the existing experiments give a poor fit and essentially exclude any solar models. Even allowing this poor fit, there is no reasonable explanation for the following constraints from the data: the  ${}^7\text{Be}$  and CNO fluxes are zero, and the  ${}^8\text{B}$  flux is about 40% of the SSM prediction; the  $pp$  flux is the maximum value allowed by the luminosity constraint:

$$\phi(pp)/\phi(pp)_{\text{SSM}} = 1.089 - 1.095 \quad (6)$$

$$\phi(\text{Be})/\phi(\text{Be})_{\text{SSM}} \leq 0.07 \quad (7)$$

$$\phi(\text{B})/\phi(\text{B})_{\text{SSM}} = 0.41 \pm 0.04 \quad (8)$$

$$\phi(\text{CNO})/\phi(\text{CNO})_{\text{SSM}} \leq 0.26, \quad (9)$$

where the uncertainties are at  $1\sigma$ ; the CNO flux includes the  ${}^{13}\text{N}$  and  ${}^{15}\text{O}$  neutrinos, which are varied with the same scale factor. When the constraints are expressed as absolute fluxes, one obtains

$$\phi(pp) = (6.53 - 6.57) \times 10^{10} \text{ cm}^{-2}\text{sec}^{-1} \quad (10)$$

$$\phi(\text{Be}) \leq 0.34 \times 10^9 \text{ cm}^{-2}\text{sec}^{-1} \quad (11)$$

$$\phi(\text{B}) = (2.33 \pm 0.23) \times 10^6 \text{ cm}^{-2}\text{sec}^{-1} \quad (12)$$

$$\phi(\text{N}) \leq 1.28 \times 10^8 \text{ cm}^{-2}\text{sec}^{-1} \quad (13)$$

$$\phi(\text{O}) \leq 1.11 \times 10^8 \text{ cm}^{-2}\text{sec}^{-1}. \quad (14)$$

This severe suppression of the  ${}^7\text{Be}$  flux relative to the  ${}^8\text{B}$  flux is inconsistent with any of the explicit nonstandard solar models. This problem is made even worse if  $S_{17}$  is lower than the values usually assumed. Even discarding any one of the three data, the constraints are consistent with the above.

When the two-flavor MSW effect is introduced in the analysis, the flux constraint from the current data is weak, but consistent with the SSM, sufficient to exclude the nonstandard models with too-small  ${}^8\text{B}$  fluxes:

$$\phi(\text{B})/\phi(\text{B})_{\text{SSM}} = 1.15 \pm 0.53 (1\sigma) \quad (15)$$

or

$$\phi(\text{B}) = (6.54 \pm 3.02) \times 10^6 \text{cm}^{-2} \text{sec}^{-1} (1\sigma) \quad (16)$$

No meaningful constraint is obtained if the other fluxes are introduced as free parameters.

We have also considered the flux constraints in the presence of two-flavor MSW by assuming various outcomes from the next generation high-counting experiments. Of course, one can always consider more complicated particle physics effects, such as three-flavor oscillations involving sterile neutrinos. Here, however, we consider the simplest scenario, expecting that, should two-flavor MSW be the case, it will be established as the most likely solution by the NC measurement in SNO, and by spectral distortions and day-night asymmetry measurements in SNO and Super-Kamiokande. Assuming hypothetical outcomes from the SNO NC and BOREXINO measurements with realistic uncertainties for this simplest scenario, we found that the  ${}^7\text{Be}$  and  ${}^8\text{B}$  fluxes will be determined at the  $\pm 20\%$  and  $\pm 15\%$  levels, making competing solar models distinguishable even if the MSW effect is operative. The MSW parameters will also be determined with sufficient accuracy independent of solar models. We emphasize that the neutral current sensitivity for  ${}^7\text{Be}$  neutrinos in BOREXINO, HELLAZ, and HERON is essential for obtaining such constraints. We did not incorporate the information from the SNO CC rate, Super-Kamiokande rate, spectral distortions, or day-night asymmetry; those data should provide more stringent constraints on the MSW parameters as well as on the fluxes. The  $pp$  flux can be measured by the HELLAZ and HERON experiments, but a measurement uncertainty at the few % level is required to determine the flux more accurately than the luminosity constraint.

## ACKNOWLEDGMENTS

We thank Eugene Beier and Sidney Bludman for useful discussions. This work is supported by the Department of Energy Contract DE-AC02-76-ERO-3071.

## REFERENCES

- \* Present address: Department of Physics, The Ohio State University, Columbus, Ohio 43210.
- [1] R. Davis, Jr. *et al.*, in *Proceedings of the 21th International Cosmic Ray Conference*, edited by R. J. Protheroe (University of Adelaide Press, Adelaide, 1990), Vol. 12, p. 143; R. Davis, Jr., in *Frontiers of Neutrino Astrophysics*, edited by Y. Suzuki and K. Nakamura (Universal Academy Press, Tokyo, 1993), P. 47.
- [2] K. Lande, in *Neutrino 94*, Eilat, Israel, May-June 1994.
- [3] Kamiokande II Collaboration, K. S. Hirata *et al.*, Phys. Rev. Lett. **65**, 1297 (1990); **65**, 1301(1990); **66**, 9 (1991); Phys. Rev. D **44**, 2241 (1991).
- [4] Y. Suzuki, in *Neutrino 94*, Eilat, Israel, May-June 1994.
- [5] SAGE Collaboration, A. I. Abazov, *et al.*, Phys. Rev. Lett. **67**, 3332 (1991); SAGE Collaboration, J. N. Abdurashitov *et al.*, Phys. Lett. B **328**, 234 (1994).
- [6] V. N. Gavrin, in *Neutrino 94*, Eilat, Israel, May-June 1994; SAGE Collaboration, J. N. Abdurashitov *et al.*, to be published in *Proceedings of the 5th Conference on the Intersection of Particle and Nuclear Physics*, St. Petersburg, Florida, May-June 1994.
- [7] GALLEX Collaboration, P. Anselmann *et al.*, Phys. Lett. B **285**, 376 (1992); **285**, 390 (1992); **314**, 445 (1993); **327**, 337 (1994).
- [8] J. N. Bahcall and M. H. Pinsonneault, Rev. Mod. Phys. **64**, 885 (1992).
- [9] S. Turck-Chièze and I. Lopes, Astrophys. J. **408**, 347 (1993). S. Turck-Chièze, S. Cahen, M. Cassé, and C. Doom, Astrophys. J. **335**, 415 (1988).
- [10] J. N. Bahcall and H. A. Bethe, Phys. Rev. D **47**, 1298 (1993); Phys. Rev. Lett. **65**, 2233 (1990); H. A. Bethe and J. N. Bahcall, Phys. Rev. D **44**, 2962 (1991).
- [11] N. Hata, S. Bludman, and P. Langacker, Phys. Rev. D **49**, 3622 (1994).

- [12] J. N. Bahcall, Phys. Rev. D **44**, 1644 (1991).
- [13] L. Wolfenstein, Phys. Rev. D **17**, 2369 (1978); **20**, 2634 (1979); S. P. Mikheyev and A. Yu. Smirnov, Yad. Fiz. **42**, 1441 (1985) [Sov. J. Nucl. Phys. **42**, 913 (1985)]; Nuovo Cimento **9C**, 17 (1986).
- [14] N. Hata and P. Langacker, Phys. Rev. D **50**, 632 (1994).
- [15] T. Motobayashi *et al.*, Report No. Rikkyo RUP 94-2, Yale 40609-1141 (submitted to Phys. Rev. Lett.)
- [16] C. W. Johnson, E. Kolbe, S. E. Koonin, and K. Langanke, Astrophys. J. **392**, 320 (1992).
- [17] G. T. Ewan *et al.* “Sudbury Neutrino Observatory Proposal”, Report No. SNO-87-12, 1987 (unpublished); “Scientific and Technical Description of the Mark II SNO Detector”, edited by E. W. Beier and D. Sinclair, Report No. SNO-89-15, 1989 (unpublished).
- [18] Y. Totsuka, University of Tokyo Report No. ICRR-Report-227-90-20, 1990 (unpublished).
- [19] J. P. Revol, in *Frontiers of Neutrino Astrophysics*, edited by Y. Suzuki and K. Nakamura (University Academy Press, Inc., Tokyo, Japan, 1993), p. 167.
- [20] “BOREXINO at Gran Sasso — proposal for a real time detector for low energy solar neutrinos”, Vol. 1, edited by G. Bellini, M. Campanella, D. Giugni, and R. Raghavan (1991).
- [21] J. Seguinot, T. Ypsilantis, and A. Zichini, College de France Report No. LPC92-31, 1992 (unpublished).
- [22] S. R. Bandler *et al.*, Journal of Low Temperature Phys. **93**, 785 (1993).
- [23] J. N. Bahcall and R. N. Ulrich, Rev. Mod. Phys. **60**, 297 (1988).



- [24] J. N. Bahcall, *Neutrino Astrophysics*, (Cambridge University Press, Cambridge, England, 1989).
- [25] S. Bludman, D. Kennedy, and P. Langacker, *Phys. Rev. D* **45**, 1810 (1992); *Nucl. Phys. B* **374**, 373 (1992).
- [26] S. Bludman, N. Hata, D. Kennedy, and P. Langacker, *Phys. Rev. D* **47**, 2220 (1993).
- [27] V. Castellani *et al.*, INFN preprint INFNFE-3-94, 1994 (unpublished).
- [28] V. Castellani, S. Degl’Innocenti, and G. Fiorentini, *Astron. Astrophys.* **271**, 601 (1993).
- [29] M. B. Aufderheide, S. D. Bloom, D. A. Resler, and C. D. Goodman, *Phys. Rev. C* **49**, 678 (1994).
- [30] J. Bahcall, Ref. [24], Table 6.6, p. 163.
- [31] D. Dearborn, private communications.
- [32] J. Faulkner and R. L. Gilliland, *Astrophys. J.* **299**, 994 (1985); R. L. Gilliland, J. Faulkner, W. H. Press, and D. N. Spergel, *Astrophys. J.* **306**, 703 (1986).
- [33] V. Castellani, S. Degl’Innocenti, and G. Fiorentini, *Phys. Lett. B* **303**, 68 (1993).
- [34] R. Sienkiewicz, J. N. Bahcall, and B. Paczyński, *Astrophys. J.* **349**, 641 (1990).
- [35] A. Dar and G. Shaviv, Technion preprint, 1994 (unpublished).
- [36] W. Merryfield, in *Solar Modelling*, edited by A. B. Balantekin and J. N. Bahcall (World Scientific, Singapore, 1994).
- [37] D. Gough and J. Toomre, *Annu. Rev. Astron. Astrophys.* **29**, 627 (1991); D. Gough, *Phil. Trans. R. Soc. Lond. A* **346**, 37 (1994).
- [38] X. Shi, D. N. Schramm, and D. S. P. Dearborn, Fermilab Report No. FERMILAB-PUB-94-122-A (Los Alamos Electronic Preprint No. astro-ph/9404006).

[39] N. Hata, University of Pennsylvania Report No. UPR-0605T, 1994 (unpublished).

[40] A. J. Baltz and J. Weneser, Brookhaven National Laboratory Report No. BNL-60387, 1994 (to be published in Phys. Rev. D).

## TABLES

TABLE I. The standard solar model predictions of Bahcall and Pinsonneault (BP SSM) [8] and of Turck-Chi  ze and Lopes (TL SSM) [9], along with the results of the solar neutrino experiments.

	BP SSM	TL SSM	Experiments
Kamiokande <sup>a</sup> ( $10^6 \text{ cm}^{-2}\text{sec}^{-1}$ )	$5.69 \pm 0.82$	$4.4 \pm 1.1$	$2.89 \pm 0.41$ ( $0.51 \pm 0.07$ BP SSM)
Homestake <sup>b</sup> (SNU)	$8 \pm 1$	$6.4 \pm 1.4$	$2.55 \pm 0.25$ ( $0.32 \pm 0.03$ BP SSM)
SAGE <sup>c</sup> & GALLEX <sup>d</sup> (SNU)	$131.5 \begin{smallmatrix} +7 \\ -6 \end{smallmatrix}$	$122.5 \pm 7$	$77 \pm 9$ ( $0.59 \pm 0.07$ BP SSM)

<sup>a</sup>The combined result of Kamiokande II and III (total of 1670 days) is  $2.89 +0.22/-0.21$  (stat)  $\pm 0.35$  (sys)  $\times 10^6 \text{ cm}^{-2}\text{sec}^{-1}$  [4].

<sup>b</sup>The result through June, 1992 (Run 18 – 124) is  $2.55 \pm 0.17$  (stat)  $\pm 0.18$  (sys) SNU [2].

<sup>c</sup>The combined result of SAGE I and II (through January, 1993) is  $74 +13/-12$  (stat)  $+5/-7$  (sys) SNU [6].

<sup>d</sup>The combined result of GALLEX I and II (30 runs, through October, 1993) is  $79 \pm 10$  (stat)  $\pm 6$  (sys) SNU [7].

TABLE II. To simplify the notation, we use the following neutrino fluxes as units. These reference fluxes correspond to the Bahcall-Pinsonneault standard solar model with the helium diffusion effect [8].

	$\text{cm}^{-2} \text{ sec}^{-1}$
$\phi(pp)_{\text{SSM}}$	$6.00 \times 10^{10}$
$\phi(pep)_{\text{SSM}}$	$1.43 \times 10^8$
$\phi(hep)_{\text{SSM}}$	$1.23 \times 10^3$
$\phi(\text{Be})_{\text{SSM}}$	$4.89 \times 10^9$
$\phi(\text{B})_{\text{SSM}}$	$5.69 \times 10^6$
$\phi(\text{N})_{\text{SSM}}$	$4.92 \times 10^8$
$\phi(\text{O})_{\text{SSM}}$	$4.26 \times 10^8$
$\phi(\text{F})_{\text{SSM}}$	$5.39 \times 10^6$

TABLE III. The constraints on fluxes from various combinations of the current data with and without the MSW effect. The uncertainties are at  $1\sigma$ , and the fluxes are in units of the reference values defined in Table II. The constraints are converted to absolute fluxes in Table IV. The upper limit on the  $pp$  flux (1.095) is due to the luminosity constraint. Without the MSW effect, we note that the constraints are consistent with each other even if any one of the three data is ignored, but are inconsistent with the SSM and nonstandard solar models, which generally suppress the  ${}^8\text{B}$  flux more than the  ${}^7\text{Be}$  flux. When the MSW effect is present, a reasonable constraint is obtained only for the  ${}^8\text{B}$  flux. The obtained flux is consistent with the SSM prediction, albeit with a large uncertainty.

	$pp$	${}^7\text{Be}$	${}^8\text{B}$	CNO
Constraints without the MSW effect				
Kam + Cl + Ga	1.089 – 1.095	$< 0.07$	$0.41 \pm 0.04$	$< 0.26$
Kam + Cl	1.084 – 1.095	$< 0.13$	$0.42 \pm 0.04$	$< 0.38$
Kam + Ga	1.085 – 1.095	$< 0.13$	$0.50 \pm 0.07$	$< 0.56$
Cl + Ga	1.082 – 1.095	$< 0.16$	$0.38 \pm 0.05$	$< 0.72$
Constraints with the MSW effect				
Kam + Cl + Ga	$< 1.095$	—	$1.15 \pm 0.53$	—

TABLE IV. The same as Table III, but in units of absolute fluxes. The  ${}^{13}\text{N}$  and  ${}^{15}\text{O}$  fluxes are varied with the same scale factor in the fits.

	$pp$ <sup>a</sup>	${}^7\text{Be}$ <sup>b</sup>	${}^8\text{B}$ <sup>c</sup>	${}^{13}\text{N}$ and ${}^{15}\text{O}$ <sup>d</sup>
Constraints without the MSW effect				
Kam + Cl + Ga	6.53 – 6.57	$< 0.34$	$2.33 \pm 0.23$	$< 1.28, < 1.11$
Kam + Cl	6.50 – 6.57	$< 0.64$	$2.39 \pm 0.23$	$< 1.87, < 1.62$
Kam + Ga	6.51 – 6.57	$< 0.64$	$2.85 \pm 0.40$	$< 2.76, < 2.39$
Cl + Ga	6.49 – 6.57	$< 0.78$	$2.16 \pm 0.28$	$< 3.54, < 3.07$
Constraints with the MSW effect				
Kam + Cl + Ga	$< 6.57$	—	$6.54 \pm 3.02$	—

<sup>a</sup>In units of  $10^{10} \text{ cm}^{-2}\text{sec}^{-1}$ .

<sup>b</sup>In units of  $10^9 \text{ cm}^{-2}\text{sec}^{-1}$ .

<sup>c</sup>In units of  $10^6 \text{ cm}^{-2}\text{sec}^{-1}$ .

<sup>d</sup>In units of  $10^8 \text{ cm}^{-2}\text{sec}^{-1}$ .

## FIGURES

FIG. 1. The constraints on the  ${}^7\text{Be}$  and  ${}^8\text{B}$  fluxes when the Kamiokande, Homestake, and the combined gallium results are fit separately. For each point in this plane, the data are fit to the  $pp$  and CNO fluxes subject to the luminosity constraint. The fluxes allowed by the Homestake and gallium result are below the dotted and dashed line, respectively. The fluxes allowed by Kamiokande is between the dot-dashed lines.

FIG. 2. The flux constraints obtained from the combined Kamiokande, Homestake, and gallium results. The constraints are shown for the (a)  ${}^7\text{Be}$ - ${}^8\text{B}$ , (b)  $pp$ - ${}^7\text{Be}$ , and (c)  $pp$ - ${}^8\text{B}$  planes. The best fit parameters are  $\phi(pp)/\phi(pp)_{\text{SSM}} = 1.095$ ,  $\phi(\text{Be})/\phi(\text{Be})_{\text{SSM}} = 0$ ,  $\phi(\text{B})/\phi(\text{B})_{\text{SSM}} = 0.41$ , and  $\phi(\text{CNO})/\phi(\text{CNO})_{\text{SSM}} = 0$  (Table III), but this fit is poor:  $\chi^2_{\text{min}}/1 \text{ d.f.} = 3.3$ , which is excluded at 93% C.L. Also displayed are the Bahcall-Pinsonneault SSM 90% region (BP-SSM) [8], the Bahcall-Ulrich Monte Carlo SSMs [23], the Turck-Chièze-Lopes (TL) SSM [9], and various nonstandard solar models (see the text). The observations are inconsistent with any of those standard and nonstandard solar models. Smaller  $S_{17}$  values decrease only the  ${}^8\text{B}$  flux [as indicated by the downward arrow in (a)], and *aggravate* the discrepancy between the combined data and nonstandard solar models.

FIG. 3. The flux constraints from the Kamiokande and gallium data, but without the Homestake result. The combined fit again indicates the larger suppression of the  ${}^7\text{Be}$  flux relative to  ${}^8\text{B}$ , consistent with the constraint including the Homestake result (Fig. 2). The C.L. contours in (a) correspond to  $\phi(\text{CNO}) = 0$ , while the nonstandard models within the 99% C.L. (the mixing models, the large  $S_{33}$  model, and the small  $S_{34}$  model) predict non-zero CNO fluxes, aggravating the disagreement with the data.

FIG. 4. The flux constraints from the Kamiokande and gallium results, but without the Homestake data, when the standard CNO flux is assumed. A non-zero CNO flux aggravates the disagreement between the data and solar model predictions.

FIG. 5. The gallium experiment results, the SSM gallium rates, and the gallium rates of nonstandard solar models which predict the  ${}^8\text{B}$  flux consistent with or close to the  ${}^8\text{B}$  flux observed in Kamiokande (see the text for details). The nonstandard solar models consistent with Kamiokande predict the gallium rate  $R_{\text{Ga}} \gtrsim 100 \text{ SNU}$ , contradicting the combined observed rate,  $77 \pm 9 \text{ SNU}$ . The MSW solution obtained from the combined Kamiokande and Homestake data predicts  $R_{\text{Ga}} < 100 \text{ SNU}$  [14], consistent with the data.

FIG. 6. The flux constraints from the Kamiokande and Homestake results, but without the gallium data. The constraints are consistent with those including the gallium data (Fig. 2).

FIG. 7. The flux constraints from the Homestake and gallium results, but without the Kamiokande data. The constraints are consistent with those including the Kamiokande data (Fig. 2).

FIG. 8. Various standard and nonstandard solar models displayed in the (a)  ${}^7\text{Be}$ - ${}^8\text{B}$ , (b)  $pp$ - ${}^7\text{Be}$  and (c)  $pp$ - ${}^8\text{B}$  flux parameter space. SNO and Super-Kamiokande will measure the  ${}^8\text{B}$  flux. The SNO NC measurement will constrain the  ${}^8\text{B}$  flux even if neutrino flavor oscillations are present. BOREXINO, HELLAZ, and HERON will measure the  ${}^7\text{Be}$  flux. HELLAZ and HERON will also be capable of measuring the  $pp$  flux. The determinations of the initial  ${}^7\text{Be}$  and  ${}^8\text{B}$  fluxes at the  $< 20\%$  level will make competing solar models distinguishable. For the  $pp$  flux, a determination at the few % level would be useful.

FIG. 9. The flux constraints when the hypothetical results from (a) the  ${}^8\text{B}$  flux measurement in SNO and Super-Kamiokande and (b) the  ${}^7\text{Be}$  flux measurement in BOREXINO (and in HELLAZ and HERON) are considered. The standard neutrino properties are assumed.

FIG. 10. The flux constraints for the combined SNO/Super-Kamiokande and BOREXINO results. The standard neutrino properties are assumed. The constraints are for (a) different SNO/Super-Kamiokande rates and (b) different BOREXINO rates.

FIG. 11. The flux constraints for various measurement uncertainties in (a) SNO/Super-Kamiokande and (b) BOREXINO. The standard neutrino properties are assumed. With the measurement uncertainties at the 10% level, one can distinguish between standard and nonstandard solar models and perhaps even constrain the SSM parameters.

FIG. 12. The flux constraint from the existing data when the MSW effect is assumed. The current data constrain  $\phi(\text{B})/\phi(\text{B})_{\text{SSM}} = 0.47 - 2.07$  (90% C.L.) as shown in Fig. 13 (a). The solar models with too small  ${}^8\text{B}$  fluxes are inconsistent with the existing data and the MSW hypothesis. The corresponding allowed MSW parameter space is displayed in Fig. 13 (b). No reasonable constraint is obtained when the fluxes other than  ${}^8\text{B}$  are used as free parameters.

FIG. 13. The MSW- $\phi(B)$  simultaneous fit to the existing data. This is a 3 parameter fit for 8 data points, including 6 Kamiokande day-night data bins (5 d.f.) (a) The  $\chi^2$  distribution as a function of  $\phi(B)$ . The current data constrain  $\phi(B)/\phi(B)_{\text{SSM}} = 1.15 \pm 0.53$  ( $1\sigma$ ). (b) The MSW allowed regions. The corresponding constraints on the  ${}^8\text{B}$  flux are displayed in Fig. 12. There is a third allowed region around  $\sin^2 2\theta \sim 1$  and  $\Delta m^2 \sim 0.5 \times 10^{-7} \text{ eV}^2$ , which is too small to be shown in the figure. Also shown is the region excluded by the Kamiokande day-night data (95% C.L., dotted line), which is independent of the  ${}^8\text{B}$  flux uncertainty. For comparison, the allowed regions obtained assuming the Bahcall-Pinsonneault SSM and its uncertainties are also shown.

FIG. 14. The MSW- $T_C$  simultaneous fit to the existing data. This is a 3 parameter fit for 8 data points, including 6 Kamiokande day-night data bins (5 d.f.) (a) The  $\chi^2$  distribution as a function of  $T_C$ . The current data constrain  $T_C = 1.00 \pm 0.03$ , consistent with the SSM ( $T_C = 1 \pm 0.006$ ). (b) The MSW allowed regions. There is a third allowed region around  $\sin^2 2\theta \sim 1$  and  $\Delta m^2 \sim 0.7 \times 10^{-7} \text{ eV}^2$ , which is too small to be shown in the figure. Also shown is the region excluded by the Kamiokande day-night data (95% C.L., dotted line), which is independent of  $T_C$ . For comparison, the allowed regions obtained assuming the Bahcall-Pinsonneault SSM and its uncertainties are also shown.

FIG. 15. The flux constraints for the MSW nonadiabatic region when the existing data plus possible results from (a) SNO and (b) BOREXINO are considered. The  $pp$ ,  ${}^7\text{Be}$ , and  ${}^8\text{B}$  fluxes are fit as free parameters subject to the luminosity constraint. These are 5 parameter fits (2 MSW parameters and 3 fluxes) to 4 data points (3 existing data plus 1 future data) with the luminosity constraint.

FIG. 16. The flux constraints when the combined existing data plus possible results from both SNO and BOREXINO are considered. The projected experimental results are motivated by the MSW small-angle (nonadiabatic) solution. The constraints are for (a) different SNO NC rates and (b) different BOREXINO rates. These are 5 parameter fits (2 MSW parameters and 3 fluxes) to 5 data points (3 existing data plus 2 future results) with the luminosity constraint.

FIG. 17. The MSW allowed region when the  $pp$ ,  ${}^7\text{Be}$ , and  ${}^8\text{B}$  fluxes are fit as free parameters with the luminosity constraint. The existing data plus the results from SNO NC and BOREXINO are used. We assume (a) different SNO NC rates with a fixed BOREXINO rate and (b) different BOREXINO rates with a fixed SNO NC rate. The constraints for the fluxes with similar assumptions are shown in Fig. 16 and 22. Using the CNO flux as an additional free parameter does not change the allowed regions significantly.

FIG. 18. The flux constraints for the MSW nonadiabatic region for various measurement uncertainties in (a) SNO and (b) BOREXINO. The existing data are also included in the fits.

FIG. 19. The flux constraint when hypothetical Super-Kamiokande results for various measurement uncertainties are included. The joint fit also includes the existing data and the hypothetical SNO NC and BOREXINO results. The MSW parameters are in the nonadiabatic region.

FIG. 20. The flux constraints when the CNO flux is used as an additional free parameter. The joint fit includes the existing data and the hypothetical SNO NC and BOREXINO results. The MSW parameters are in the nonadiabatic region.

FIG. 21. Same as Fig. 15, but the MSW parameters are in the large-angle region.

FIG. 22. Same as Fig. 16, but the MSW parameters are in the large-angle region.

FIG. 23. The constraints for  $T_C$  and  $S_{17}$  in the presence of MSW oscillations when the existing data plus both hypothetical SNO NC and BOREXINO results are considered. This is a 4 parameter fit (2 MSW parameters plus  $T_C$  and  $S_{17}$ ) to 5 data points (3 existing data plus 2 hypothetical results) with the luminosity constraint.



This figure "fig1-1.png" is available in "png" format from:

<http://arxiv.org/ps/hep-ph/9409372v1>

This figure "fig1-2.png" is available in "png" format from:

<http://arxiv.org/ps/hep-ph/9409372v1>

This figure "fig1-3.png" is available in "png" format from:

<http://arxiv.org/ps/hep-ph/9409372v1>

This figure "fig1-4.png" is available in "png" format from:

<http://arxiv.org/ps/hep-ph/9409372v1>

This figure "fig1-5.png" is available in "png" format from:

<http://arxiv.org/ps/hep-ph/9409372v1>

This figure "fig1-6.png" is available in "png" format from:

<http://arxiv.org/ps/hep-ph/9409372v1>

This figure "fig1-7.png" is available in "png" format from:

<http://arxiv.org/ps/hep-ph/9409372v1>

This figure "fig1-8.png" is available in "png" format from:

<http://arxiv.org/ps/hep-ph/9409372v1>



This figure "fig1-9.png" is available in "png" format from:

<http://arxiv.org/ps/hep-ph/9409372v1>

This figure "fig1-10.png" is available in "png" format from:

<http://arxiv.org/ps/hep-ph/9409372v1>

This figure "fig1-11.png" is available in "png" format from:

<http://arxiv.org/ps/hep-ph/9409372v1>

This figure "fig1-12.png" is available in "png" format from:

<http://arxiv.org/ps/hep-ph/9409372v1>

This figure "fig1-13.png" is available in "png" format from:

<http://arxiv.org/ps/hep-ph/9409372v1>

This figure "fig1-14.png" is available in "png" format from:

<http://arxiv.org/ps/hep-ph/9409372v1>

This figure "fig1-15.png" is available in "png" format from:

<http://arxiv.org/ps/hep-ph/9409372v1>

This figure "fig1-16.png" is available in "png" format from:

<http://arxiv.org/ps/hep-ph/9409372v1>



This figure "fig1-17.png" is available in "png" format from:

<http://arxiv.org/ps/hep-ph/9409372v1>

This figure "fig1-18.png" is available in "png" format from:

<http://arxiv.org/ps/hep-ph/9409372v1>

This figure "fig1-19.png" is available in "png" format from:

<http://arxiv.org/ps/hep-ph/9409372v1>

This figure "fig1-20.png" is available in "png" format from:

<http://arxiv.org/ps/hep-ph/9409372v1>

This figure "fig1-21.png" is available in "png" format from:

<http://arxiv.org/ps/hep-ph/9409372v1>

This figure "fig1-22.png" is available in "png" format from:

<http://arxiv.org/ps/hep-ph/9409372v1>

This figure "fig1-23.png" is available in "png" format from:

<http://arxiv.org/ps/hep-ph/9409372v1>

This figure "fig1-24.png" is available in "png" format from:

<http://arxiv.org/ps/hep-ph/9409372v1>



This figure "fig1-25.png" is available in "png" format from:

<http://arxiv.org/ps/hep-ph/9409372v1>

This figure "fig1-26.png" is available in "png" format from:

<http://arxiv.org/ps/hep-ph/9409372v1>

This figure "fig1-27.png" is available in "png" format from:

<http://arxiv.org/ps/hep-ph/9409372v1>

This figure "fig1-28.png" is available in "png" format from:

<http://arxiv.org/ps/hep-ph/9409372v1>

This figure "fig1-29.png" is available in "png" format from:

<http://arxiv.org/ps/hep-ph/9409372v1>

FIGURES

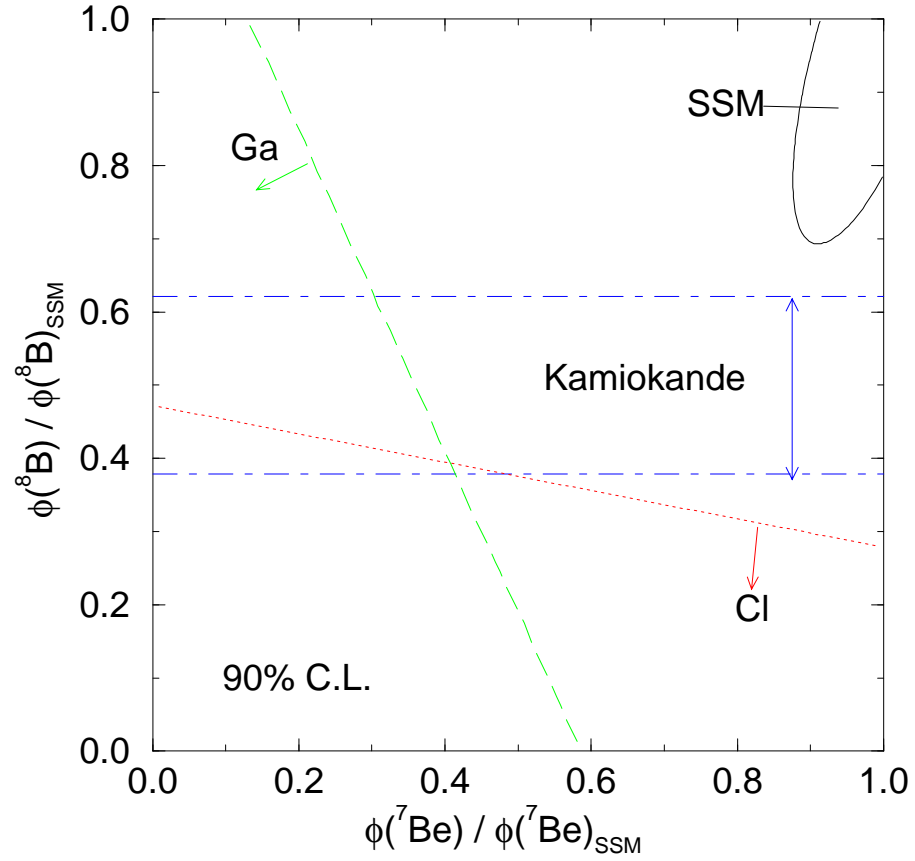
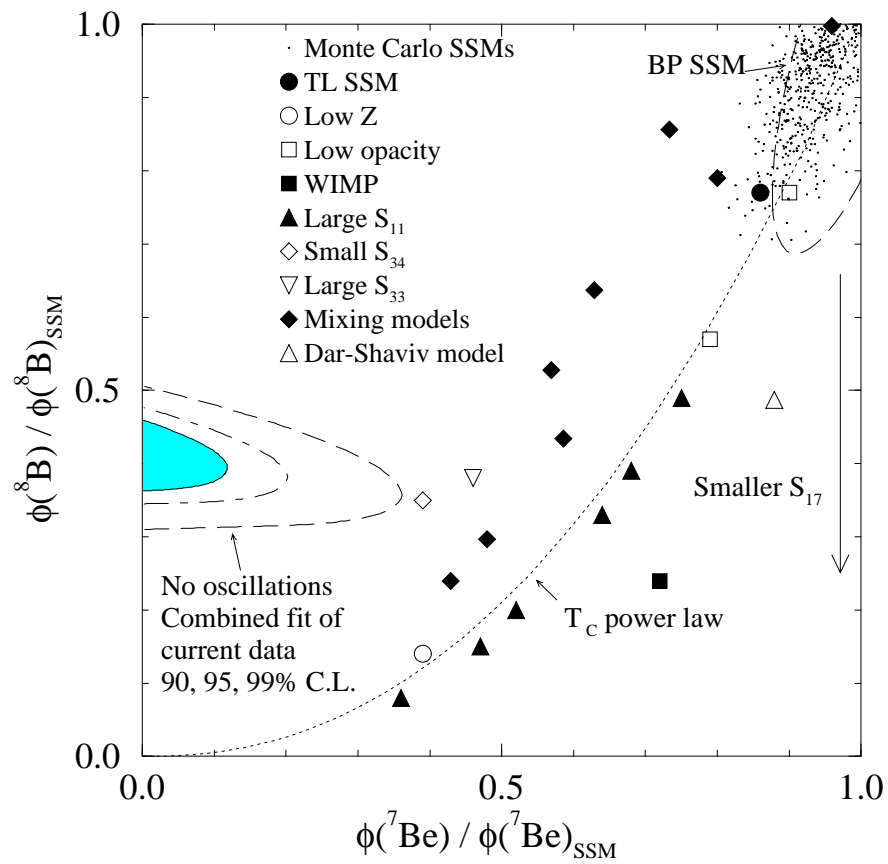
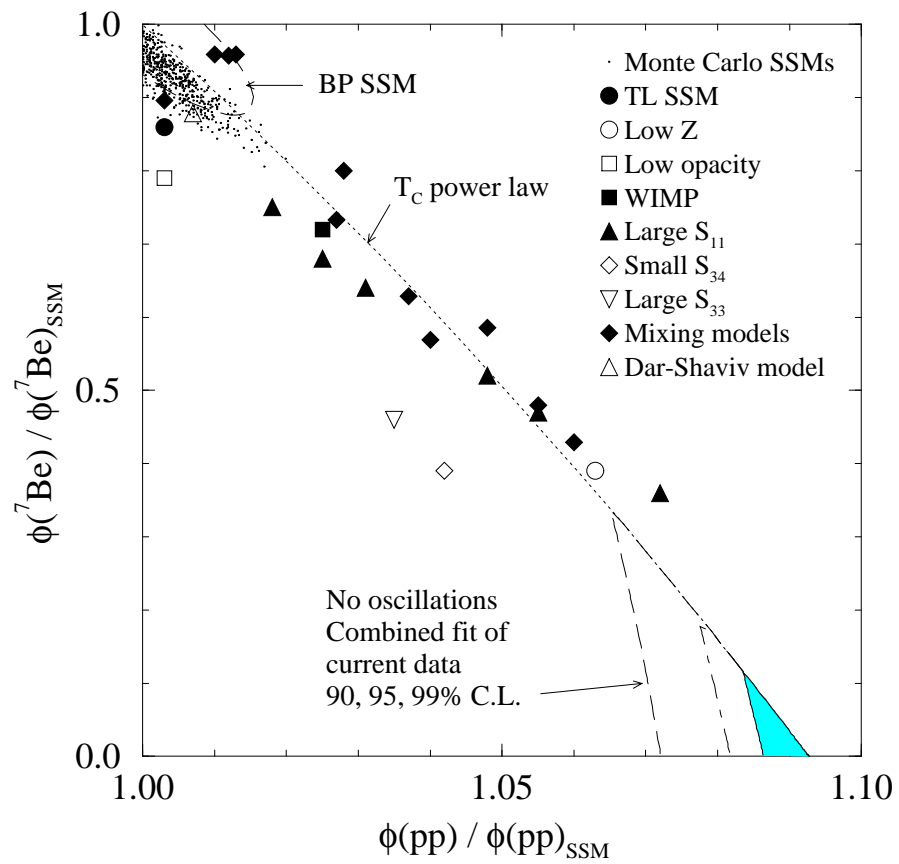


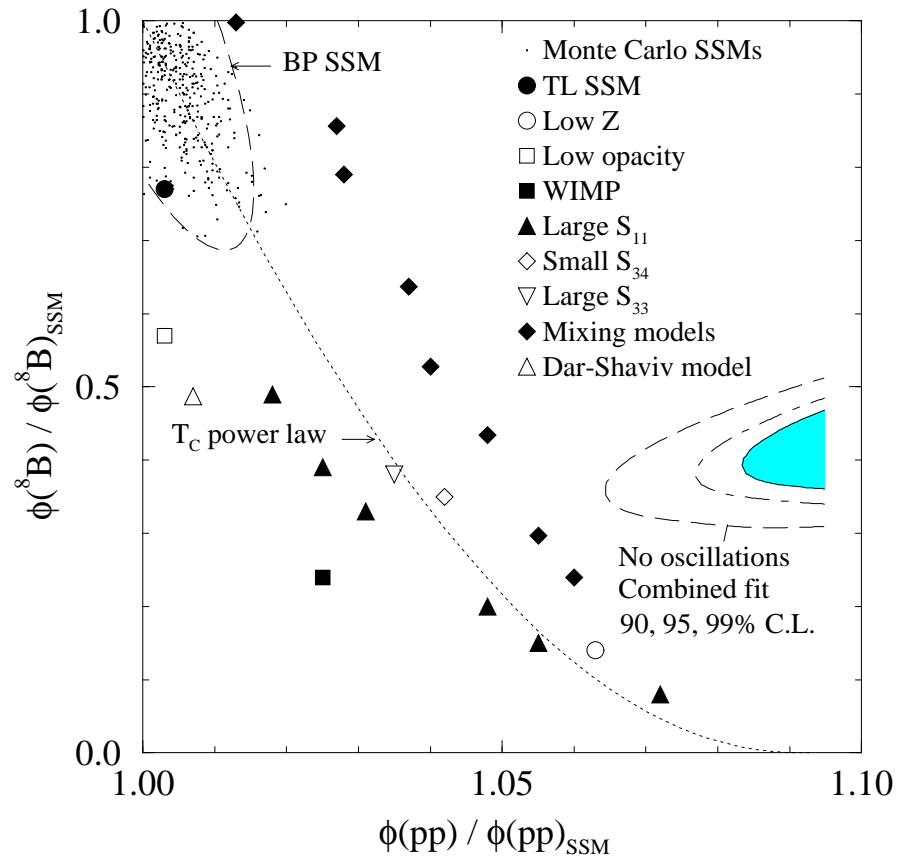
FIG. 1. The constraints on the  ${}^7\text{Be}$  and  ${}^8\text{B}$  fluxes when the Kamiokande, Homestake, and the combined gallium results are fit separately. For each point in this plane, the data are fit to the  $pp$  and CNO fluxes subject to the luminosity constraint. The fluxes allowed by the Homestake and gallium result are below the dotted and dashed line, respectively. The fluxes allowed by Kamiokande is between the dot-dashed lines.



(a)  ${}^7\text{Be}-{}^8\text{B}$



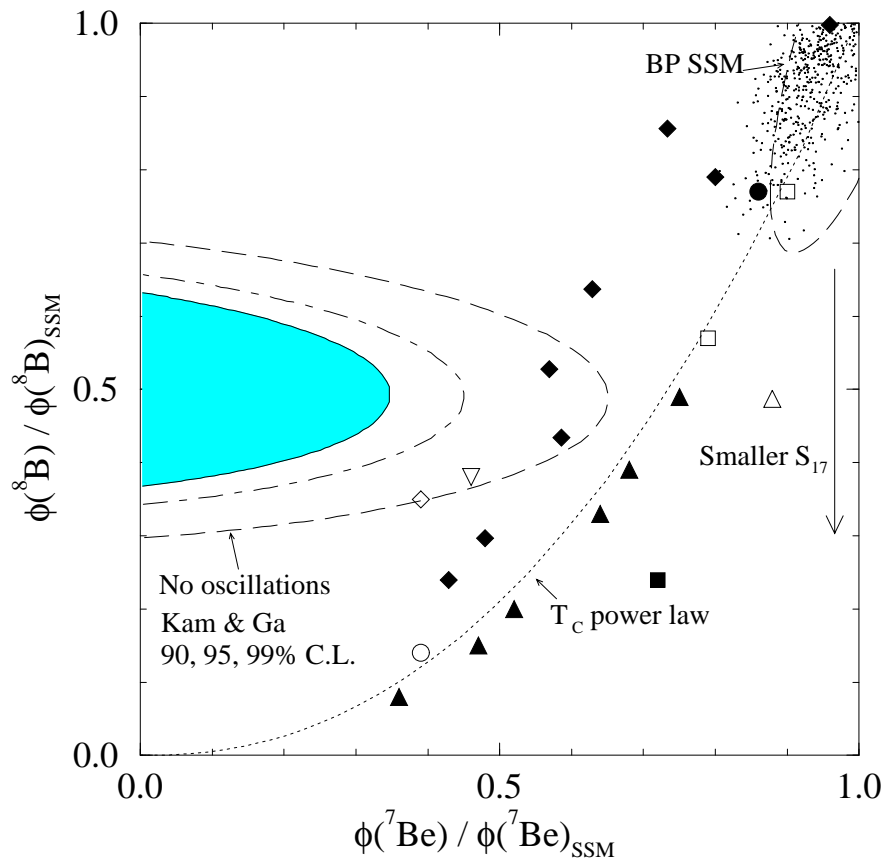
(b)  $pp-{}^7\text{Be}$



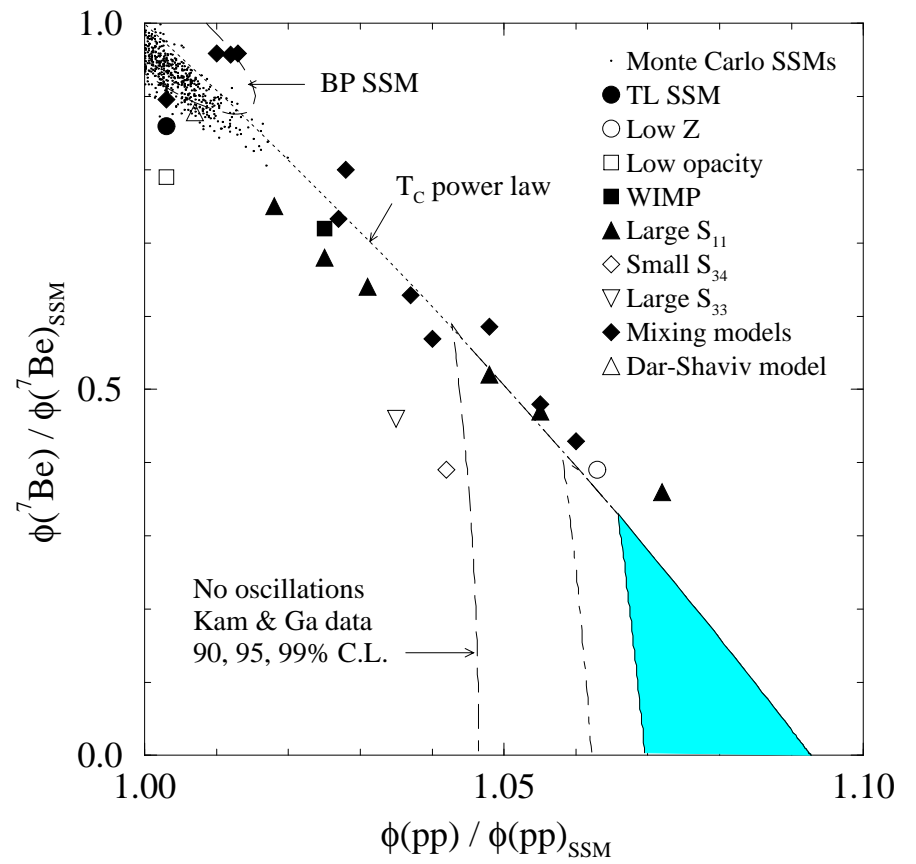
(c)  $pp\text{-}^8\text{B}$

FIG. 2. The flux constraints obtained from the combined Kamiokande, Homestake, and gallium results. The constraints are shown for the (a)  $^7\text{Be}\text{-}^8\text{B}$ , (b)  $pp\text{-}^7\text{Be}$ , and (c)  $pp\text{-}^8\text{B}$  planes. The best fit parameters are  $\phi(pp)/\phi(pp)_{SSM} = 1.095$ ,  $\phi(\text{Be})/\phi(\text{Be})_{SSM} = 0$ ,  $\phi(\text{B})/\phi(\text{B})_{SSM} = 0.41$ , and  $\phi(\text{CNO})/\phi(\text{CNO})_{SSM} = 0$  (Table III), but this fit is poor:  $\chi^2_{\min}/1 \text{ d.f.} = 3.3$ , which is excluded at 93% C.L. Also displayed are the Bahcall-Pinsonneault SSM 90% region (BP-SSM) [8], the Bahcall-Ulrich Monte Carlo SSMs [23], the Turck-Chièze-Lopes (TL) SSM [9], and various nonstandard solar models (see the text). The observations are inconsistent with any of those standard and nonstandard solar models. Smaller  $S_{17}$  values decrease only the  $^8\text{B}$  flux [as indicated by the downward arrow in (a)], and *aggravate* the discrepancy between the combined data and nonstandard solar models.

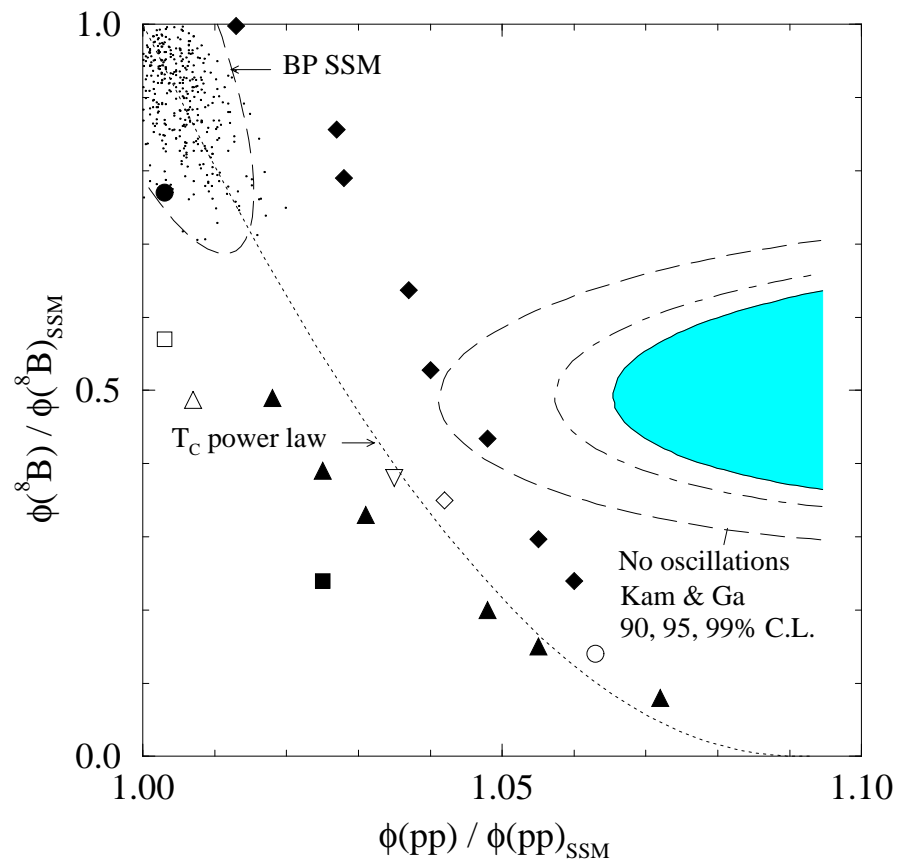




(a)  ${}^7\text{Be}-{}^8\text{B}$

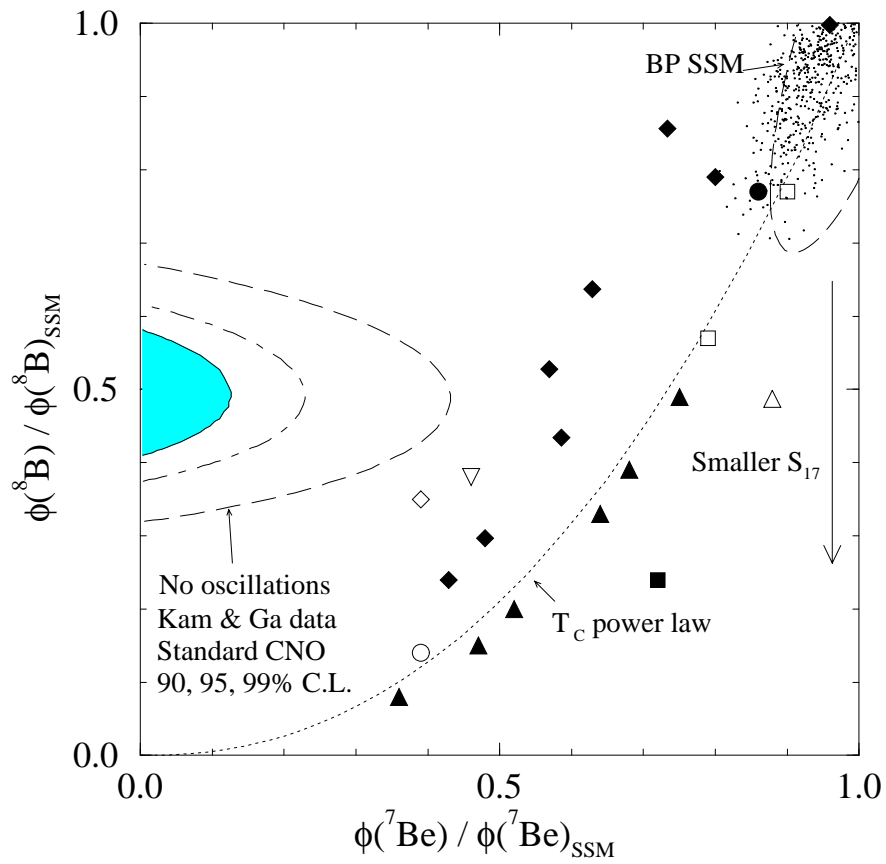


(b)  $pp-{}^7\text{Be}$

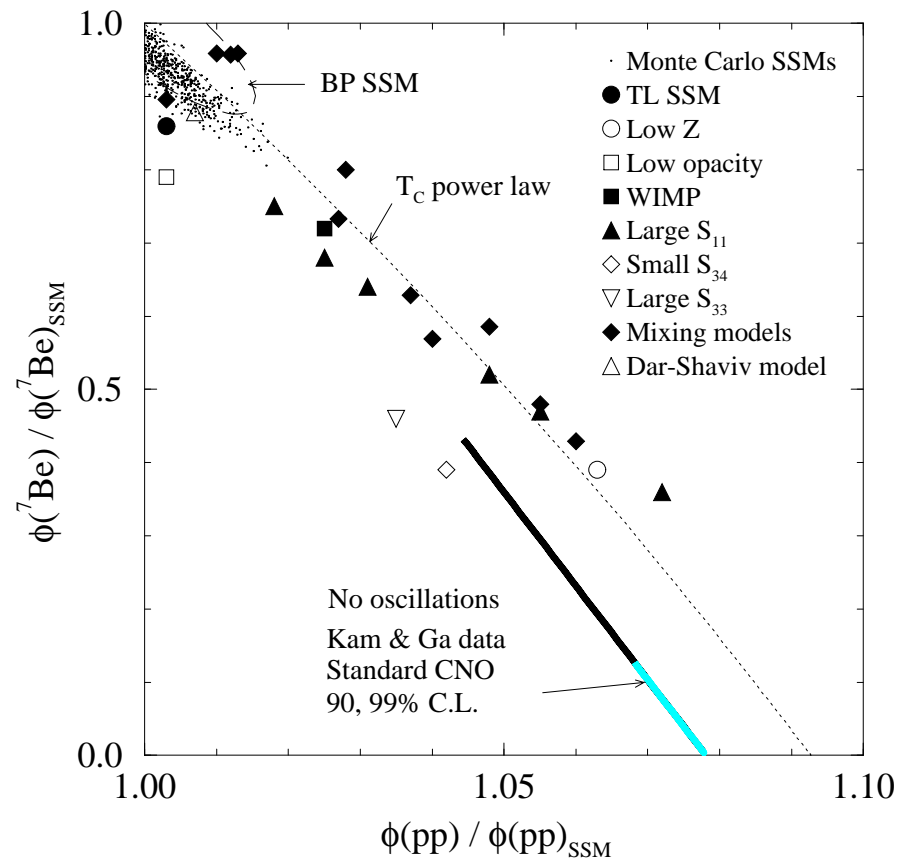


(c)  $pp$ - $^8\text{B}$

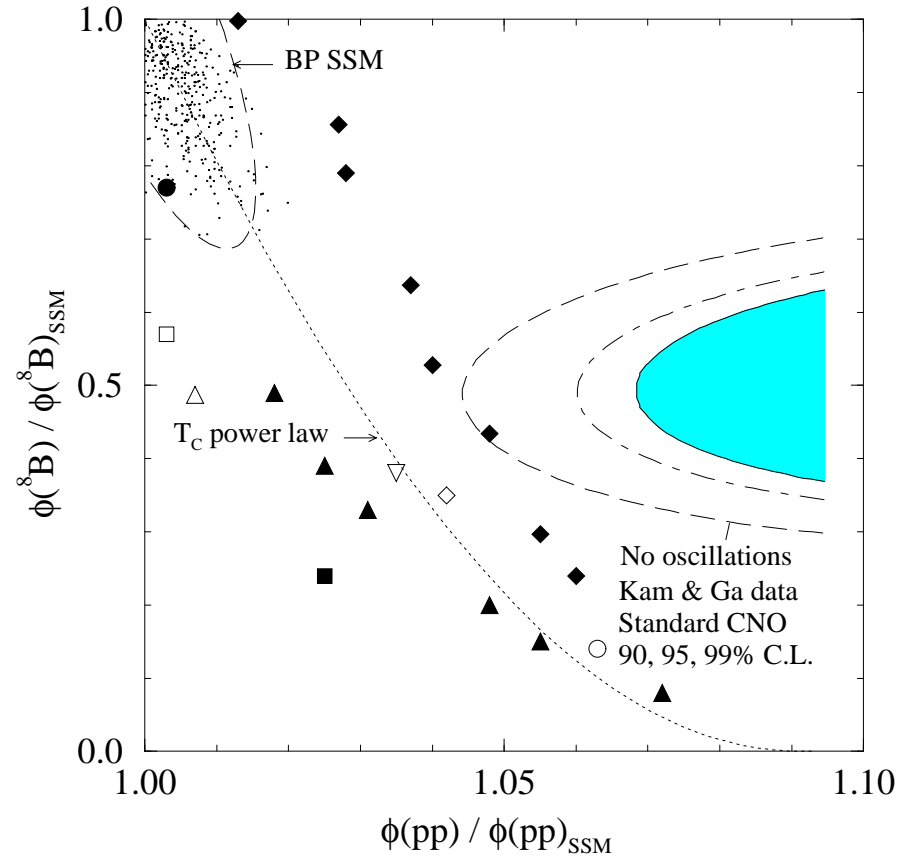
FIG. 3. The flux constraints from the Kamiokande and gallium data, but without the Homestake result. The combined fit again indicates the larger suppression of the  $^7\text{Be}$  flux relative to  $^8\text{B}$ , consistent with the constraint including the Homestake result (Fig. 2). The C.L. contours in (a) correspond to  $\phi(\text{CNO}) = 0$ , while the nonstandard models within the 99% C.L. (the mixing models, the large  $S_{33}$  model, and the small  $S_{34}$  model) predict non-zero CNO fluxes, aggravating the disagreement with the data.



(a)  ${}^7\text{Be}$ - ${}^8\text{B}$



(b)  $pp$ - ${}^7\text{Be}$



(c)  $pp\text{-}^8\text{B}$

FIG. 4. The flux constraints from the Kamiokande and gallium results, but without the Homestake data, when the standard CNO flux is assumed. A non-zero CNO flux aggravates the disagreement between the data and solar model predictions.

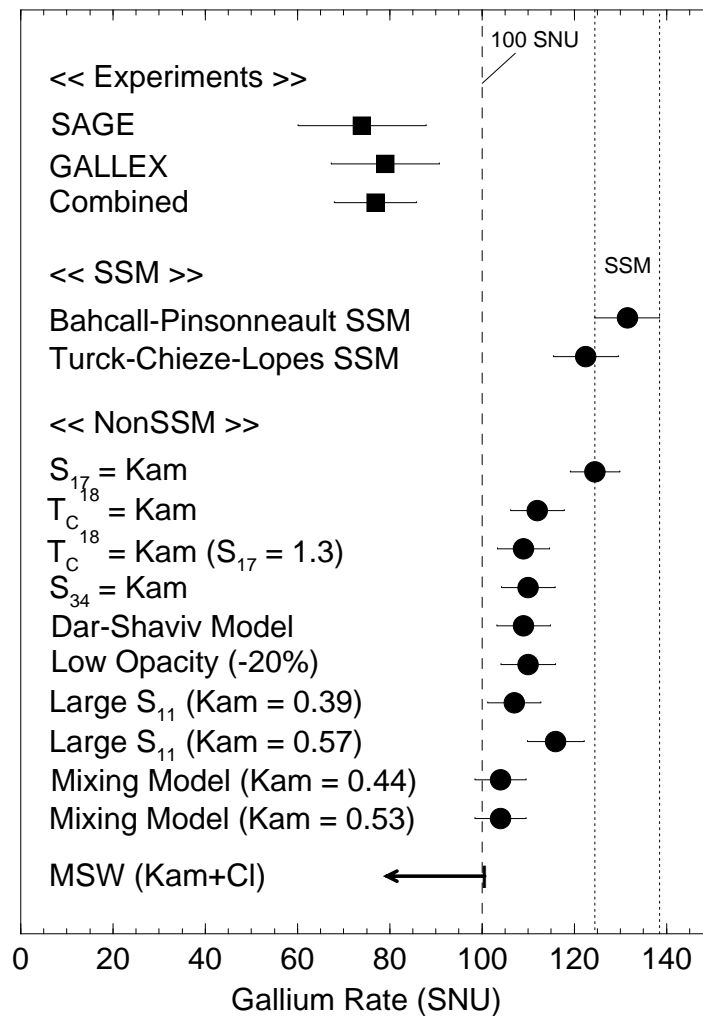
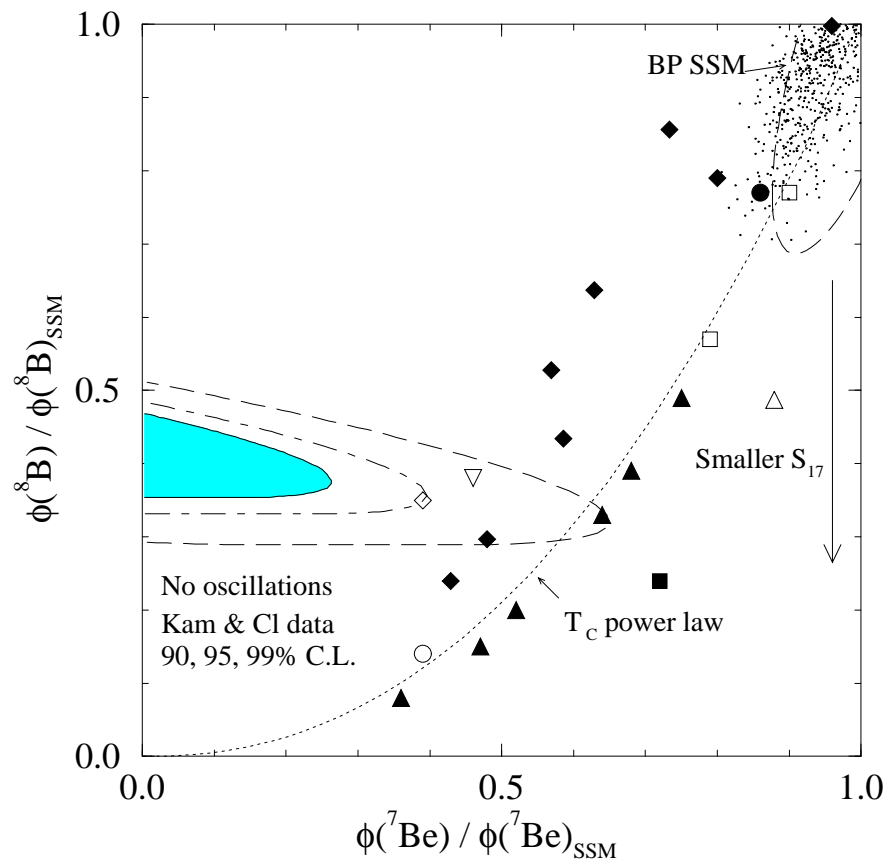
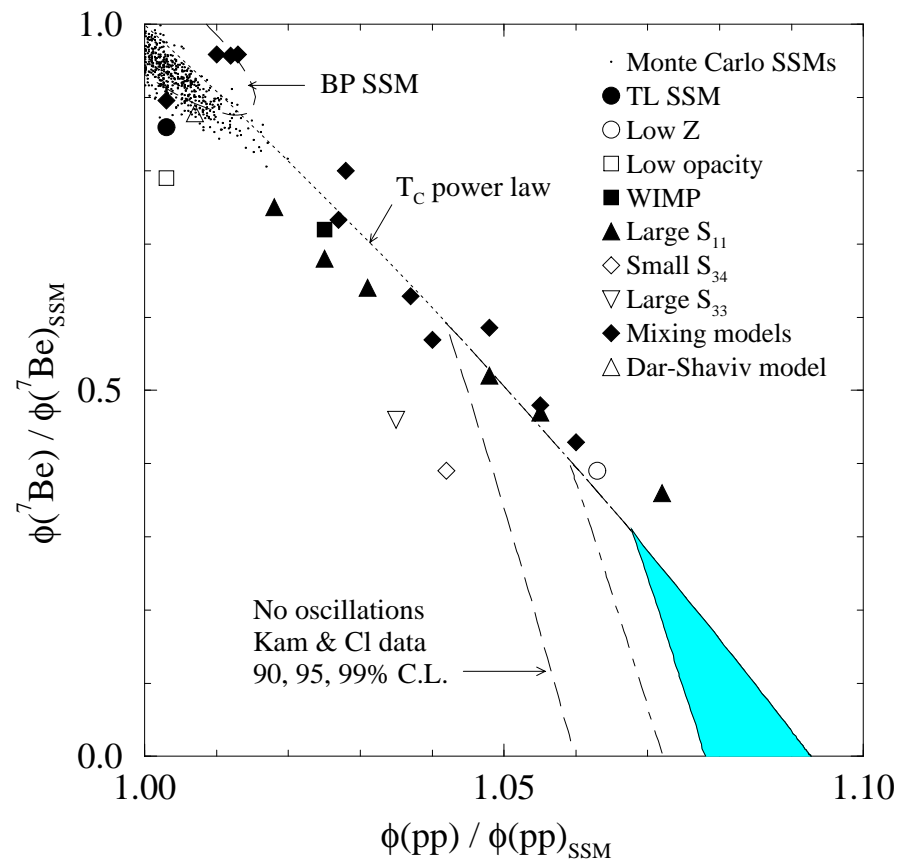


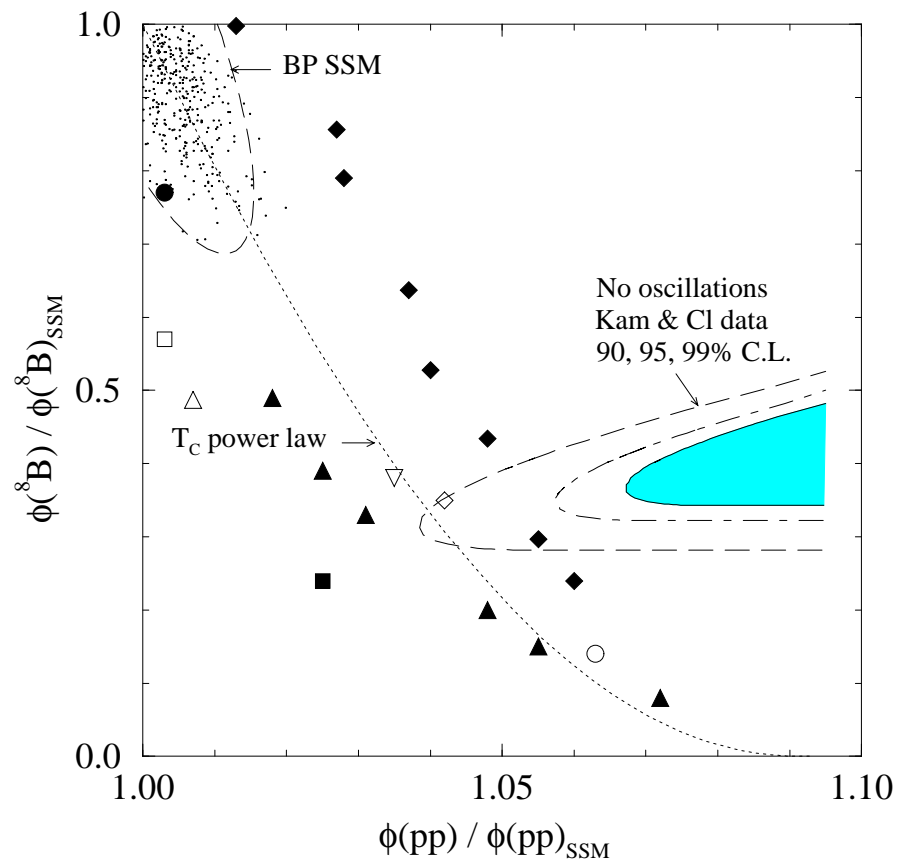
FIG. 5. The gallium experiment results, the SSM gallium rates, and the gallium rates of nonstandard solar models which predict the  ${}^8\text{B}$  flux consistent with or close to the  ${}^8\text{B}$  flux observed in Kamiokande (see the text for details). The nonstandard solar models consistent with Kamiokande predict the gallium rate  $R_{\text{Ga}} \gtrsim 100$  SNU, contradicting the combined observed rate,  $77 \pm 9$  SNU. The MSW solution obtained from the combined Kamiokande and Homestake data predicts  $R_{\text{Ga}} < 100$  SNU [14], consistent with the data.



(a)  ${}^7\text{Be}-{}^8\text{B}$

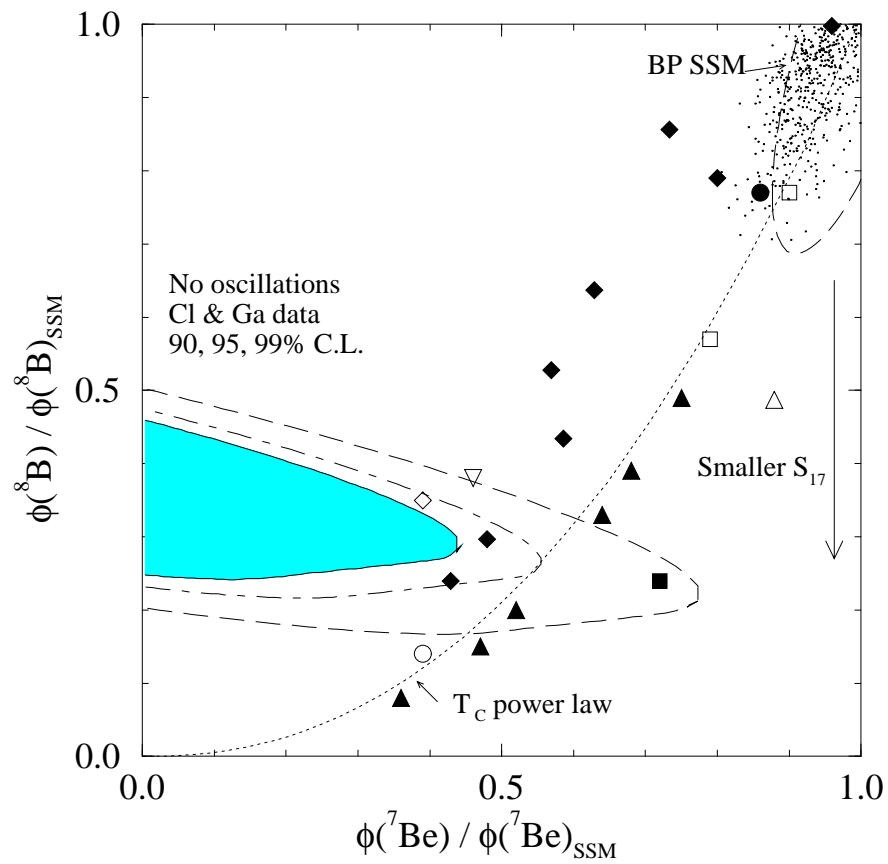


(b)  $pp-{}^7\text{Be}$

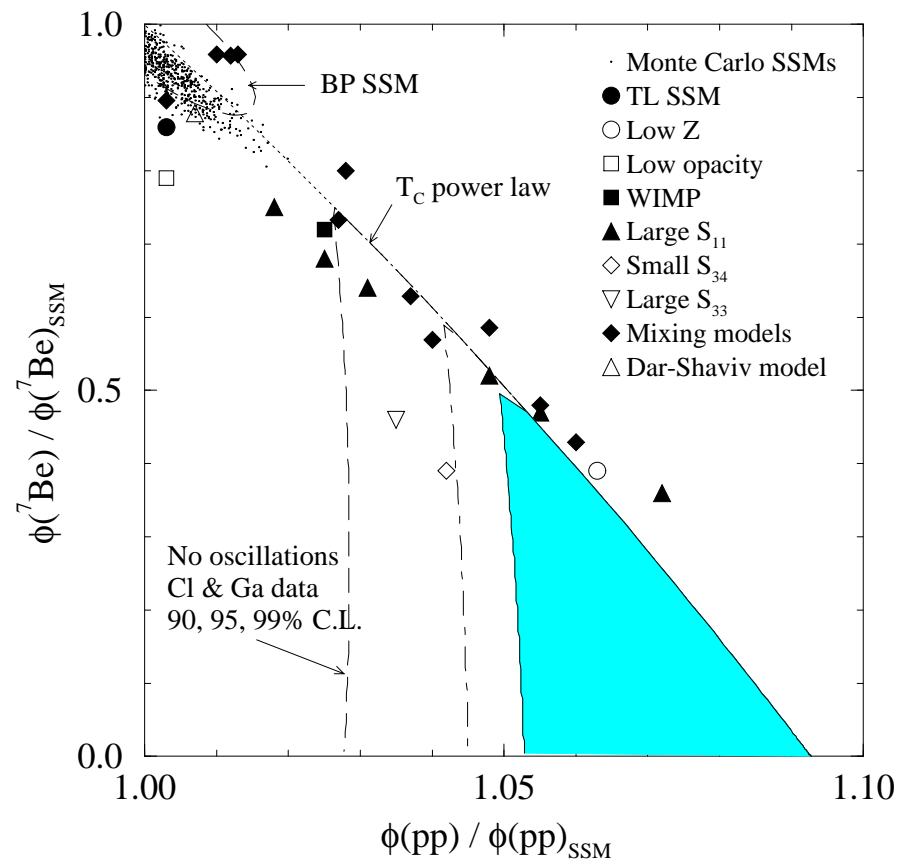


(c)  $pp\text{-}^8\text{B}$

FIG. 6. The flux constraints from the Kamiokande and Homestake results, but without the gallium data. The constraints are consistent with those including the gallium data (Fig. 2).

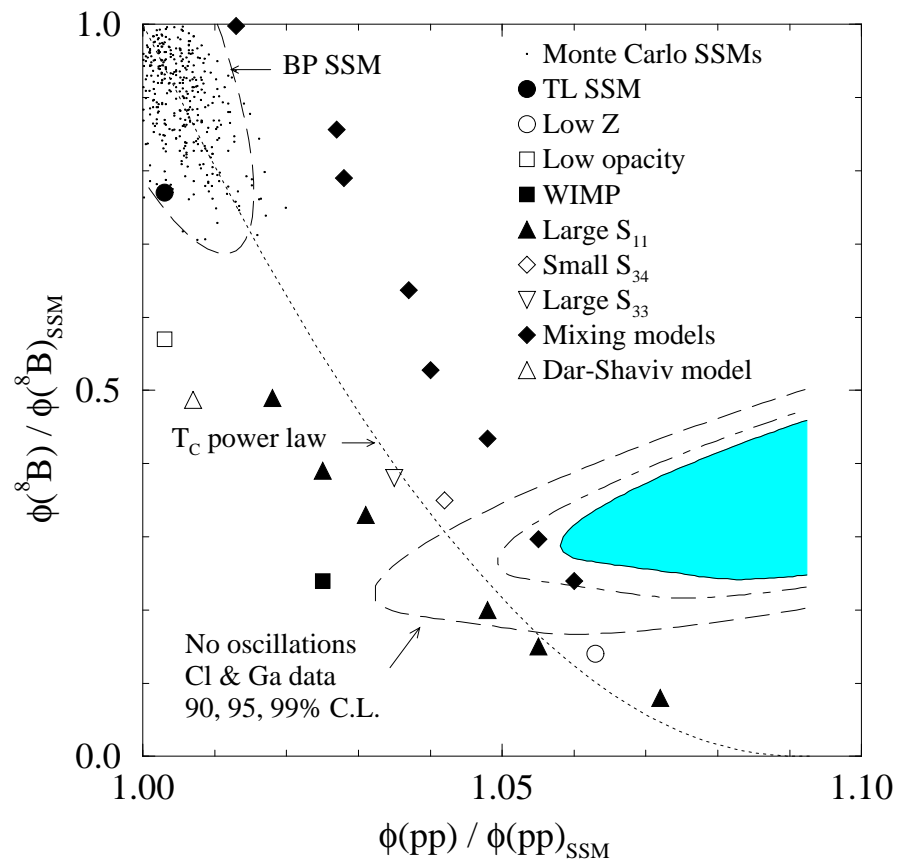


(a)  ${}^7\text{Be}-{}^8\text{B}$



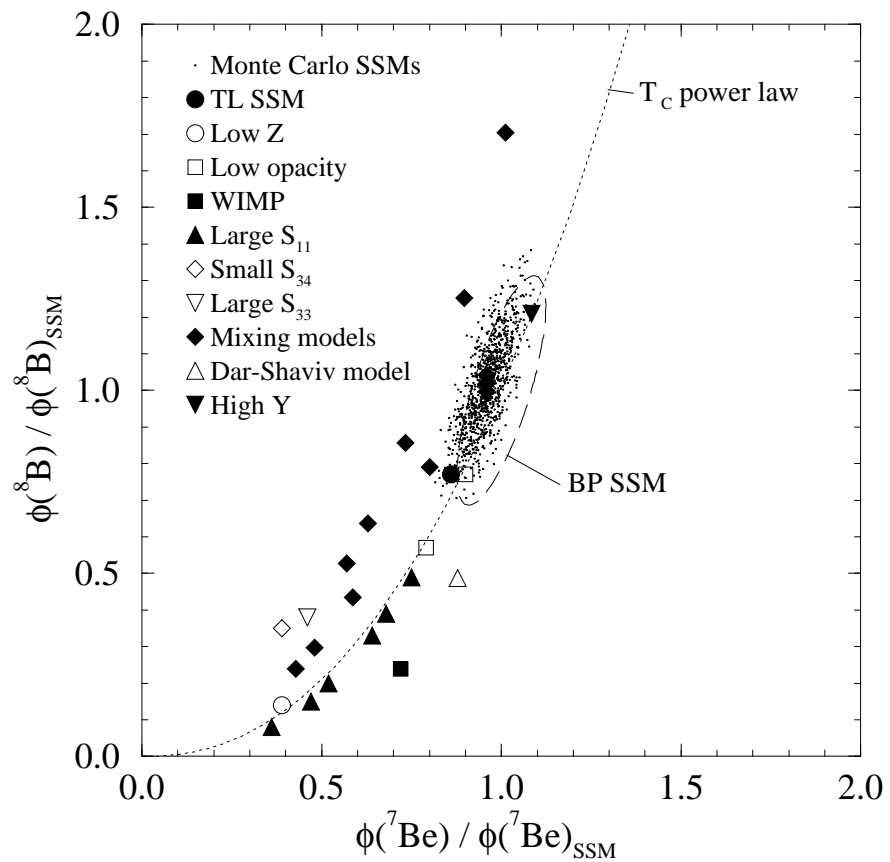
(b)  $pp-{}^7\text{Be}$



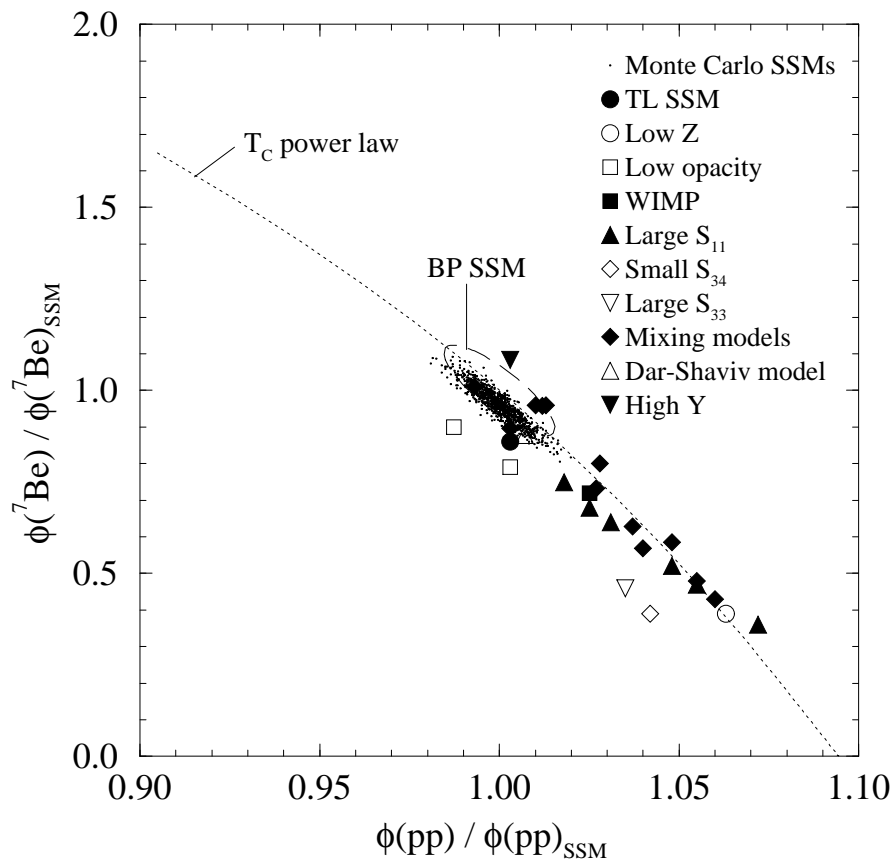


(c)  $pp\text{-}^8\text{B}$

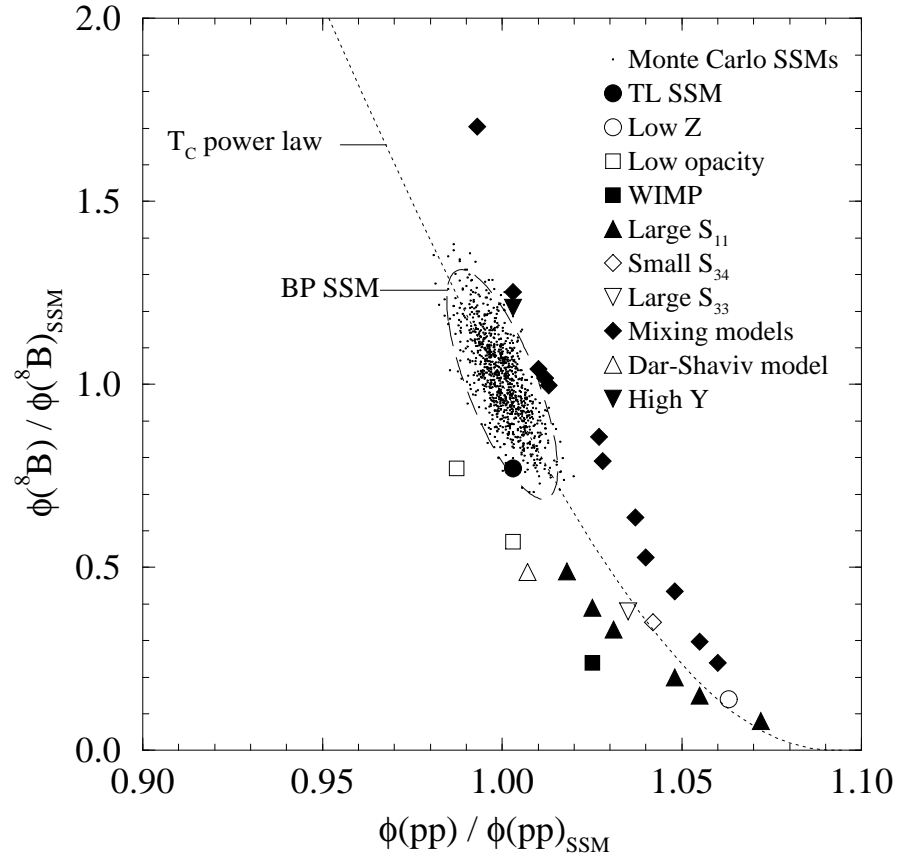
FIG. 7. The flux constraints from the Homestake and gallium results, but without the Kamiokande data. The constraints are consistent with those including the Kamiokande data (Fig. 2).



(a)  ${}^7\text{Be}$ - ${}^8\text{B}$

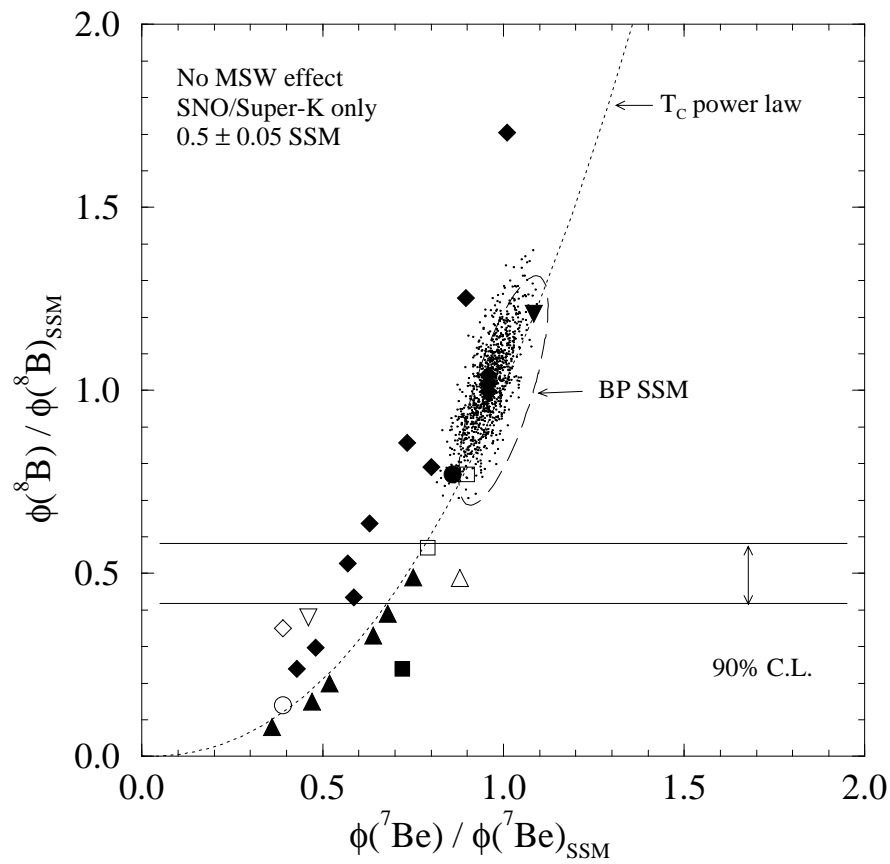


(b)  $pp$ - ${}^7\text{Be}$

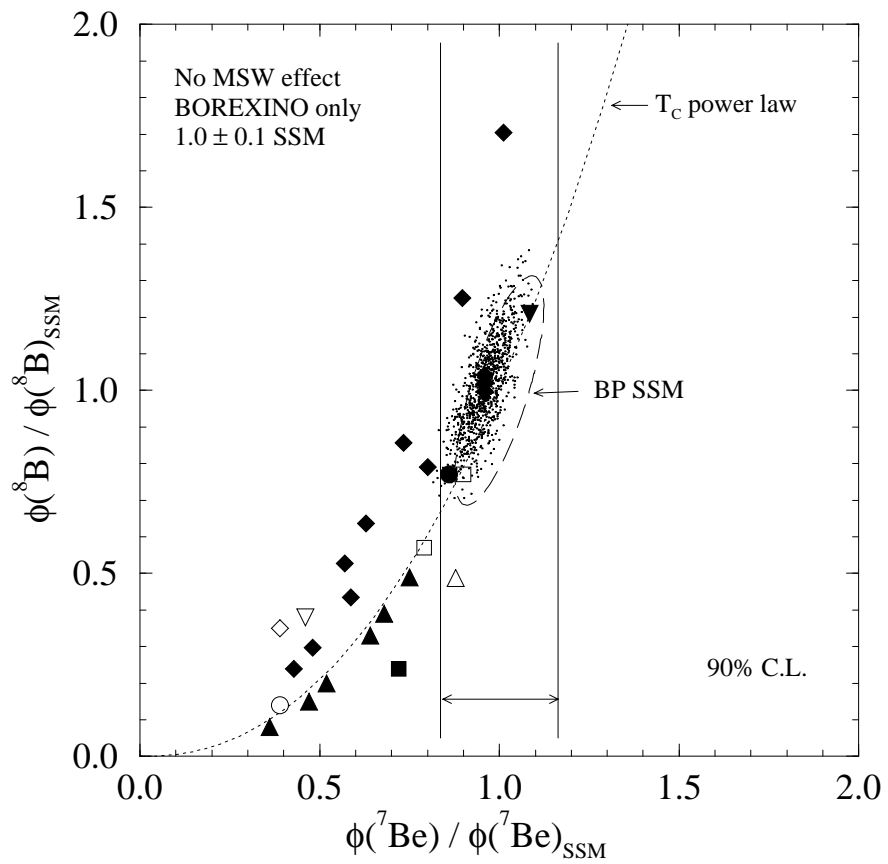


(c)  $pp$ - ${}^8\text{B}$

FIG. 8. Various standard and nonstandard solar models displayed in the (a)  ${}^7\text{Be}$ - ${}^8\text{B}$ , (b)  $pp$ - ${}^7\text{Be}$  and (c)  $pp$ - ${}^8\text{B}$  flux parameter space. SNO and Super-Kamiokande will measure the  ${}^8\text{B}$  flux. The SNO NC measurement will constrain the  ${}^8\text{B}$  flux even if neutrino flavor oscillations are present. BOREXINO, HELLAZ, and HERON will measure the  ${}^7\text{Be}$  flux. HELLAZ and HERON will also be capable of measuring the  $pp$  flux. The determinations of the initial  ${}^7\text{Be}$  and  ${}^8\text{B}$  fluxes at the  $< 20\%$  level will make competing solar models distinguishable. For the  $pp$  flux, a determination at the few % level would be useful.

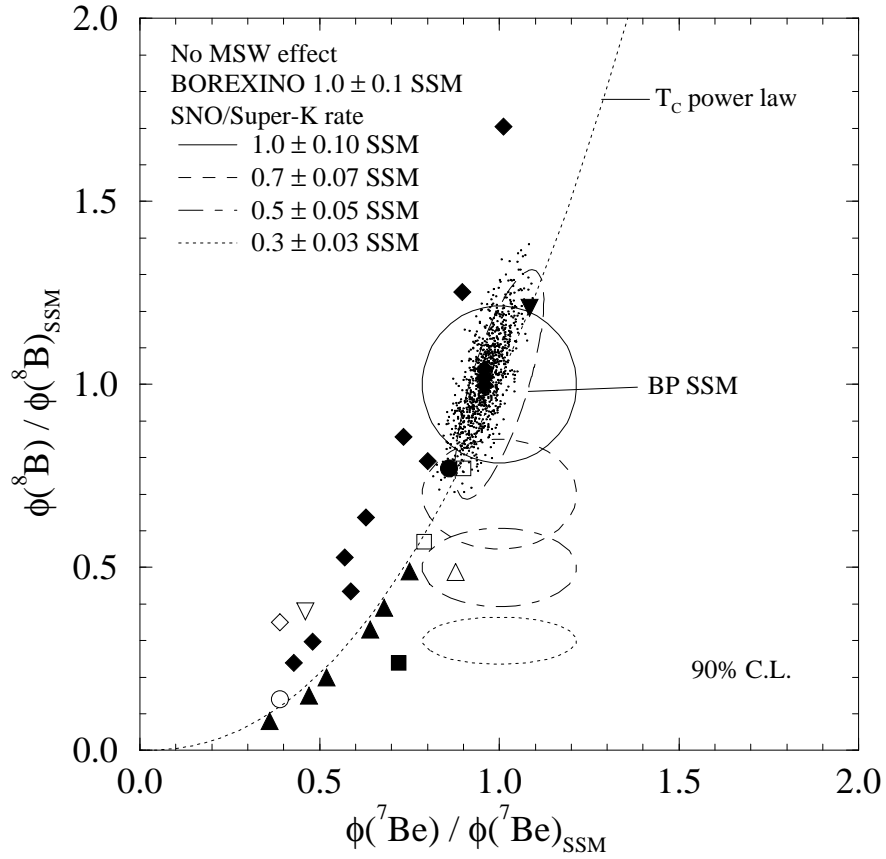


(a) SNO NC

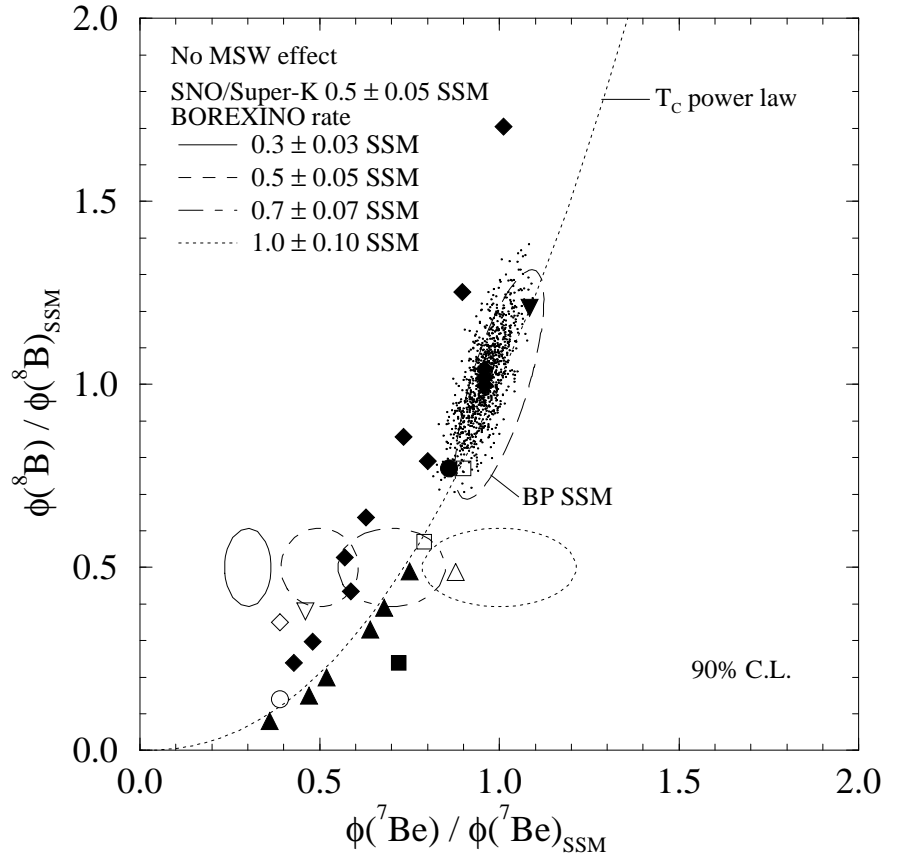


(b) BOREXINO

FIG. 9. The flux constraints when the hypothetical results from (a) the  $^8\text{B}$  flux measurement in SNO and Super-Kamiokande and (b) the  $^7\text{Be}$  flux measurement in BOREXINO (and in HELLAZ and HERON) are considered. The standard neutrino properties are assumed.

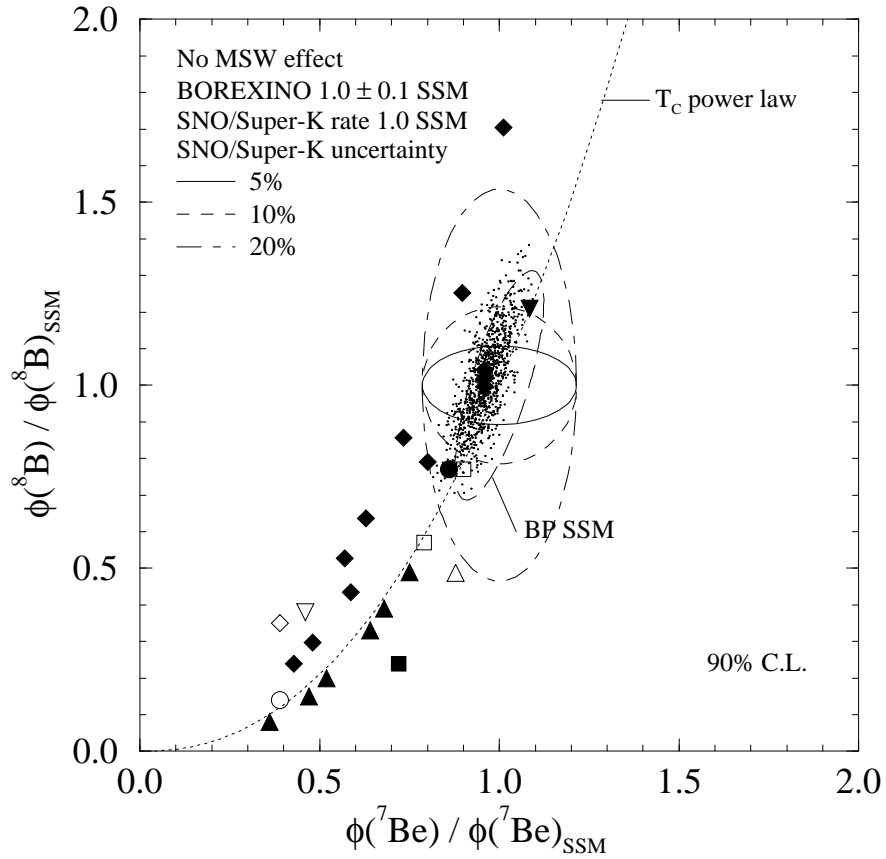


(a) Different SNO NC values

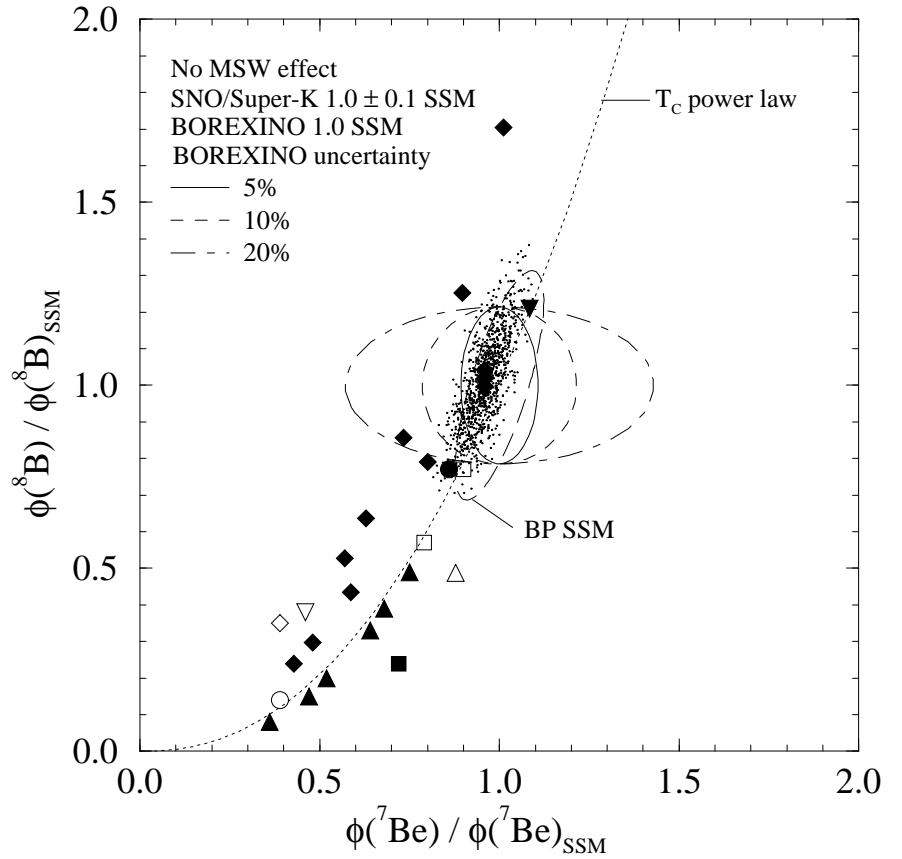


(b) Different BOREXINO values

FIG. 10. The flux constraints for the combined SNO/Super-Kamiokande and BOREXINO results. The standard neutrino properties are assumed. The constraints are for (a) different SNO/Super-Kamiokande rates and (b) different BOREXINO rates.



(a) Sensitivity for SNO/Super-K uncertainty



(b) Sensitivity for BOREXINO uncertainty

FIG. 11. The flux constraints for various measurement uncertainties in (a) SNO/Super-Kamiokande and (b) BOREXINO. The standard neutrino properties are assumed. With the measurement uncertainties at the 10% level, one can distinguish between standard and nonstandard solar models and perhaps even constrain the SSM parameters.

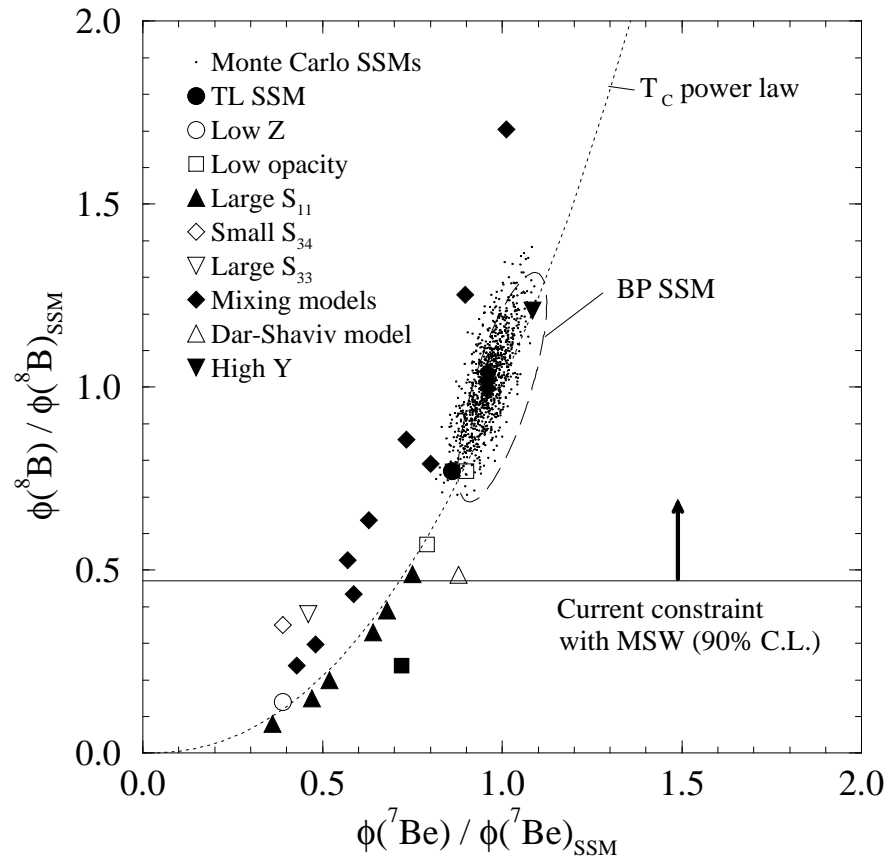


FIG. 12. The flux constraint from the existing data when the MSW effect is assumed. The current data constrain  $\phi(\text{B})/\phi(\text{B})_{\text{SSM}} = 0.47 - 2.07$  (90% C.L.) as shown in Fig. 13 (a). The solar models with too small  $^8\text{B}$  fluxes are inconsistent with the existing data and the MSW hypothesis. The corresponding allowed MSW parameter space is displayed in Fig. 13 (b). No reasonable constraint is obtained when the fluxes other than  $^8\text{B}$  are used as free parameters.

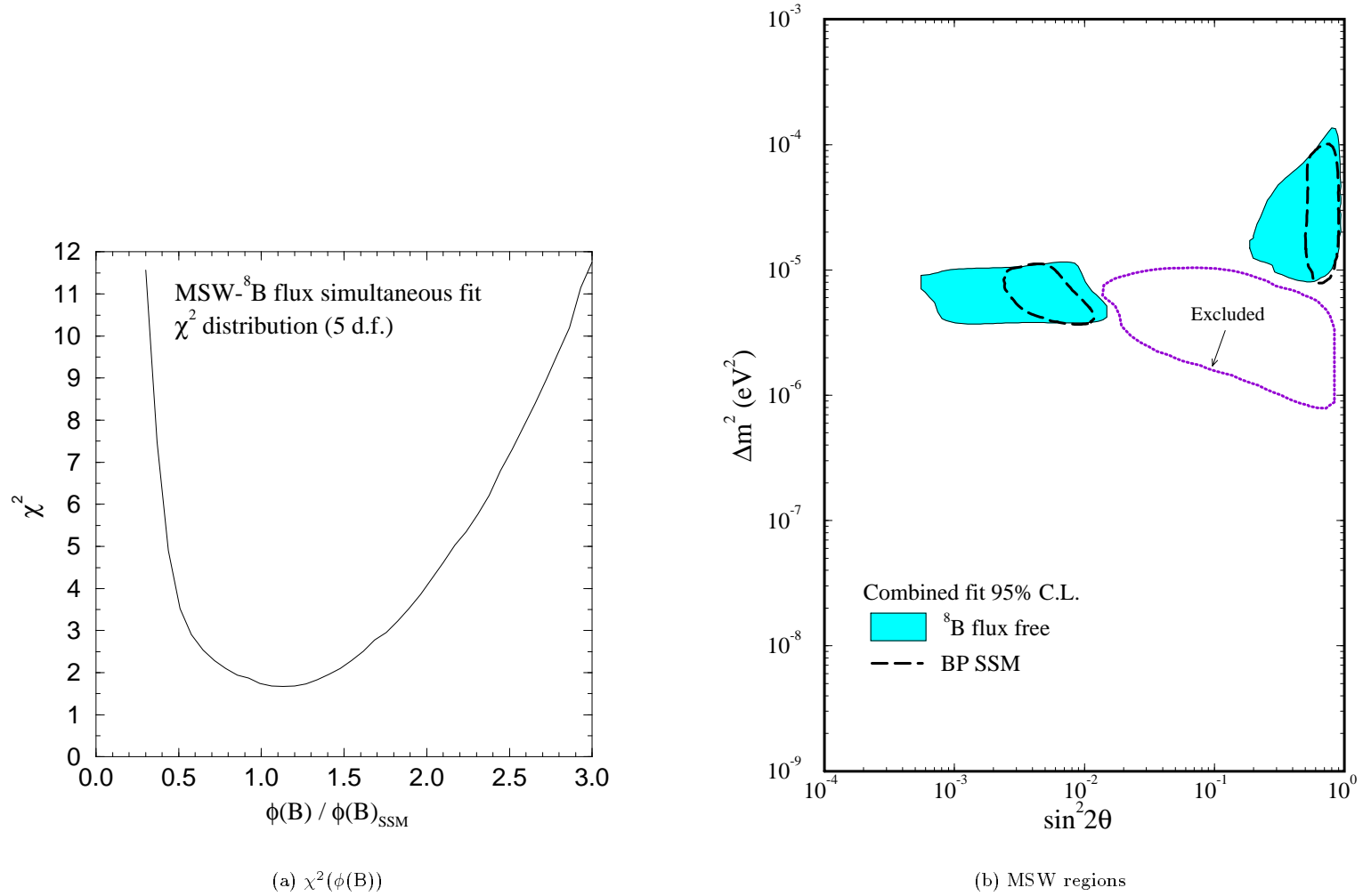


FIG. 13. The MSW- $\phi(\text{B})$  simultaneous fit to the existing data. This is a 3 parameter fit for 8 data points, including 6 Kamiokande day-night data bins (5 d.f.) (a) The  $\chi^2$  distribution as a function of  $\phi(\text{B})$ . The current data constrain  $\phi(\text{B})/\phi(\text{B})_{\text{SSM}} = 1.15 \pm 0.53$  ( $1\sigma$ ). (b) The MSW allowed regions. The corresponding constraints on the  $^8\text{B}$  flux are displayed in Fig. 12. There is a third allowed region around  $\sin^2 2\theta \sim 1$  and  $\Delta m^2 \sim 0.5 \times 10^{-7}$  eV $^2$ , which is too small to be shown in the figure. Also shown is the region excluded by the Kamiokande day-night data (95% C.L., dotted line), which is independent of the  $^8\text{B}$  flux uncertainty. For comparison, the allowed regions obtained assuming the Bahcall-Pinsonneault SSM and its uncertainties are also shown.



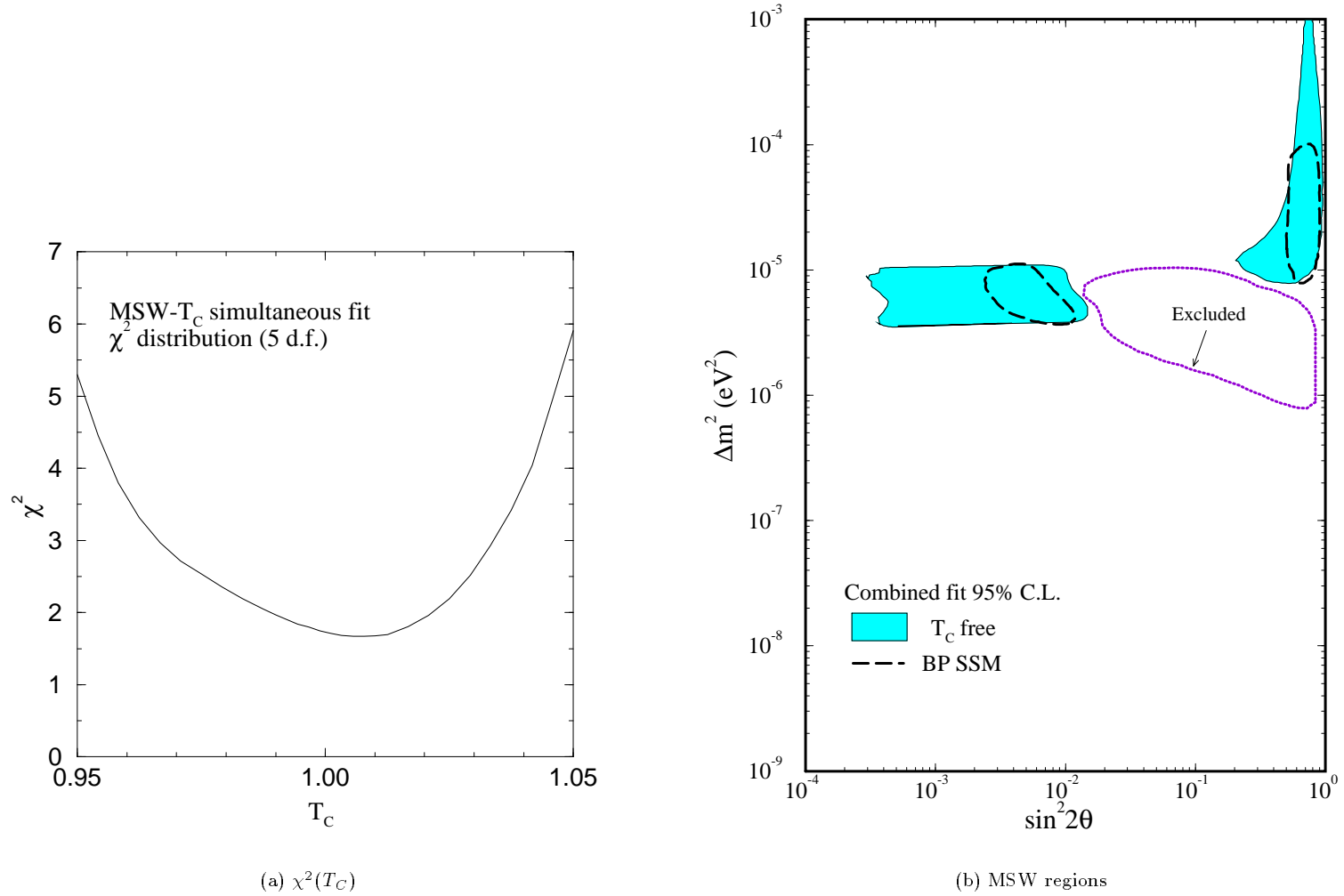
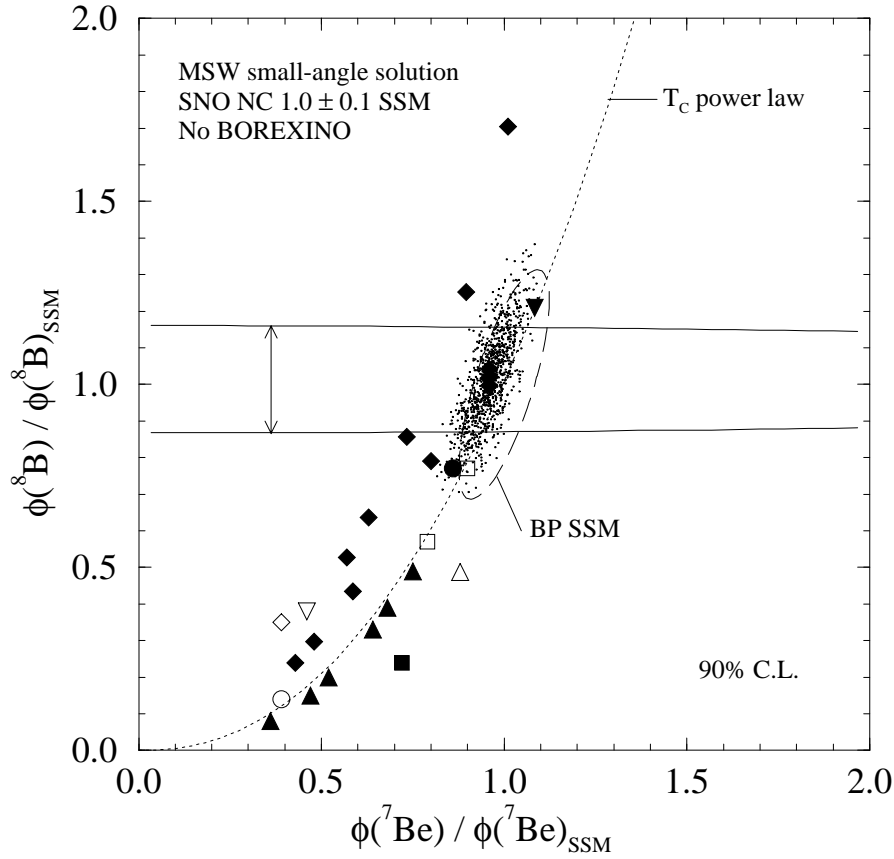
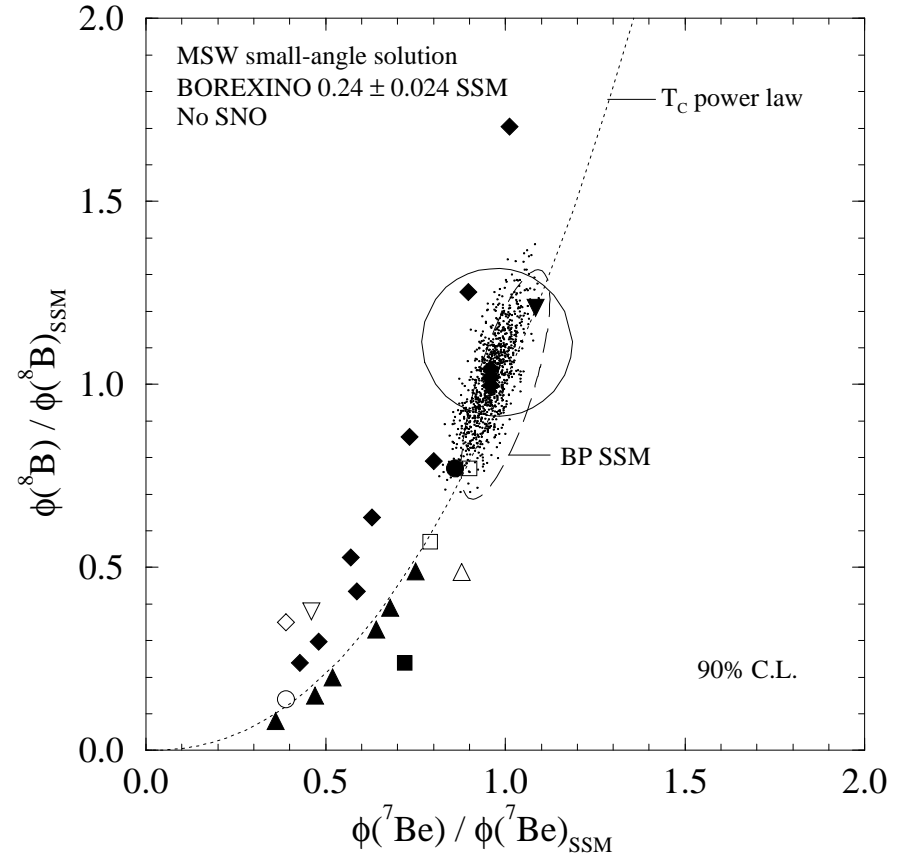


FIG. 14. The MSW- $T_C$  simultaneous fit to the existing data. This is a 3 parameter fit for 8 data points, including 6 Kamiokande day-night data bins (5 d.f.) (a) The  $\chi^2$  distribution as a function of  $T_C$ . The current data constrain  $T_C = 1.00 \pm 0.03$ , consistent with the SSM ( $T_C = 1 \pm 0.006$ ). (b) The MSW allowed regions. There is a third allowed region around  $\sin^2 2\theta \sim 1$  and  $\Delta m^2 \sim 0.7 \times 10^{-7}$  eV<sup>2</sup>, which is too small to be shown in the figure. Also shown is the region excluded by the Kamiokande day-night data (95% C.L., dotted line), which is independent of  $T_C$ . For comparison, the allowed regions obtained assuming the Bahcall-Pinsonneault SSM and its uncertainties are also shown.

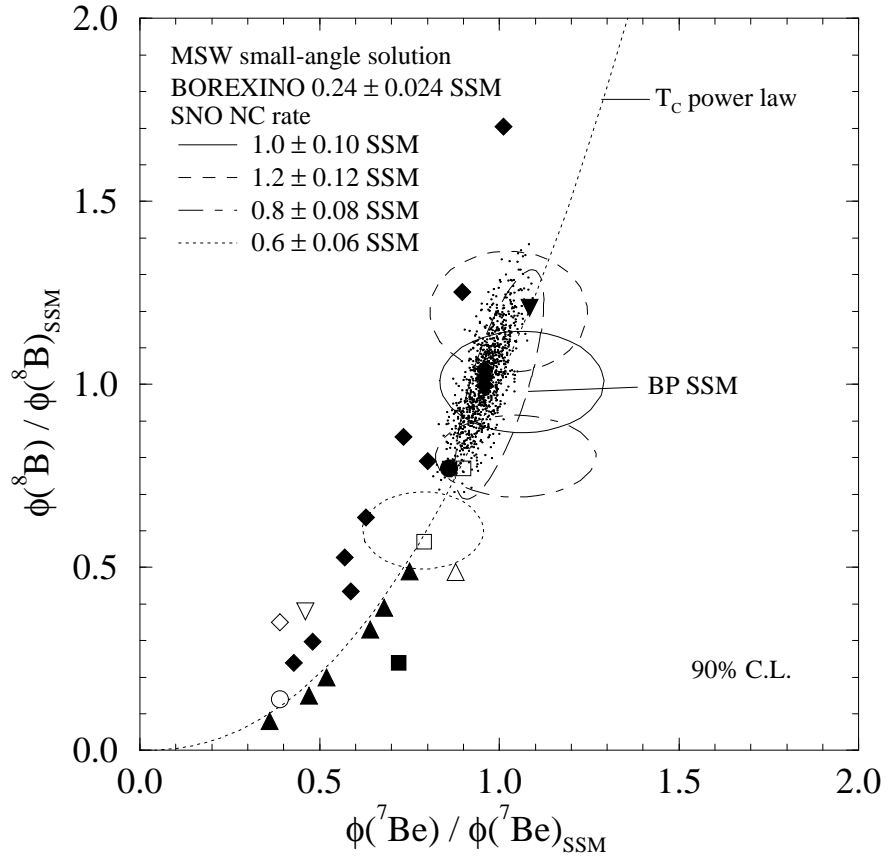


(a) SNO NC

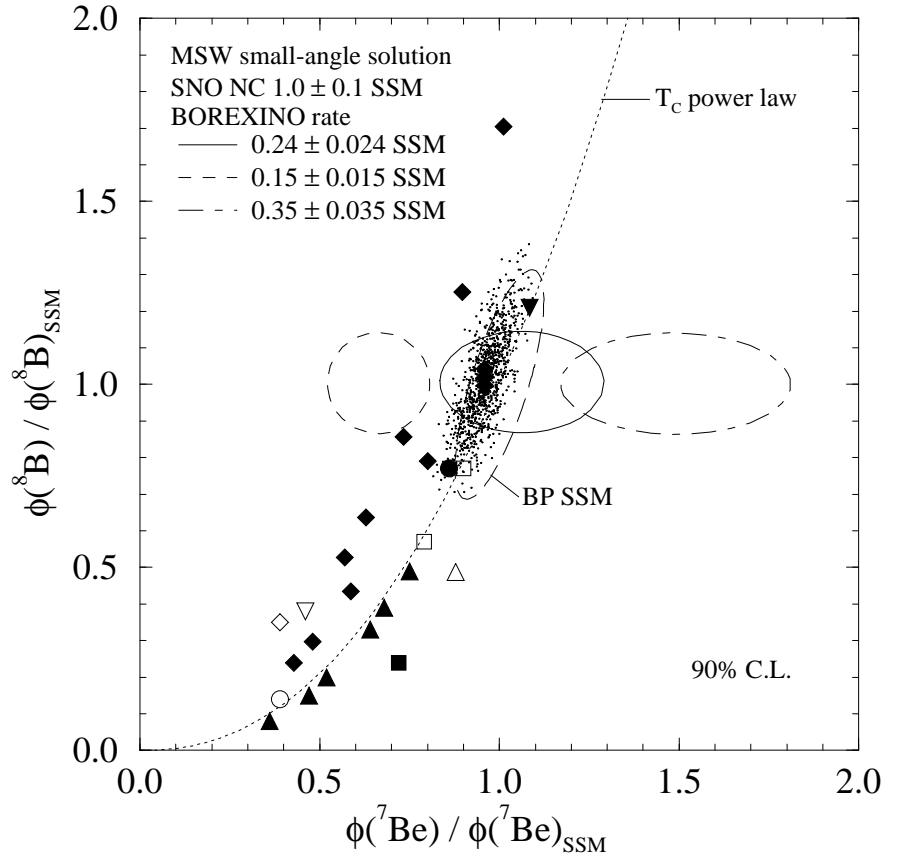


(b) BOREXINO

FIG. 15. The flux constraints for the MSW nonadiabatic region when the existing data plus possible results from (a) SNO and (b) BOREXINO are considered. The  $pp$ ,  ${}^7\text{Be}$ , and  ${}^8\text{B}$  fluxes are fit as free parameters subject to the luminosity constraint. These are 5 parameter fits (2 MSW parameters and 3 fluxes) to 4 data points (3 existing data plus 1 future data) with the luminosity constraint.

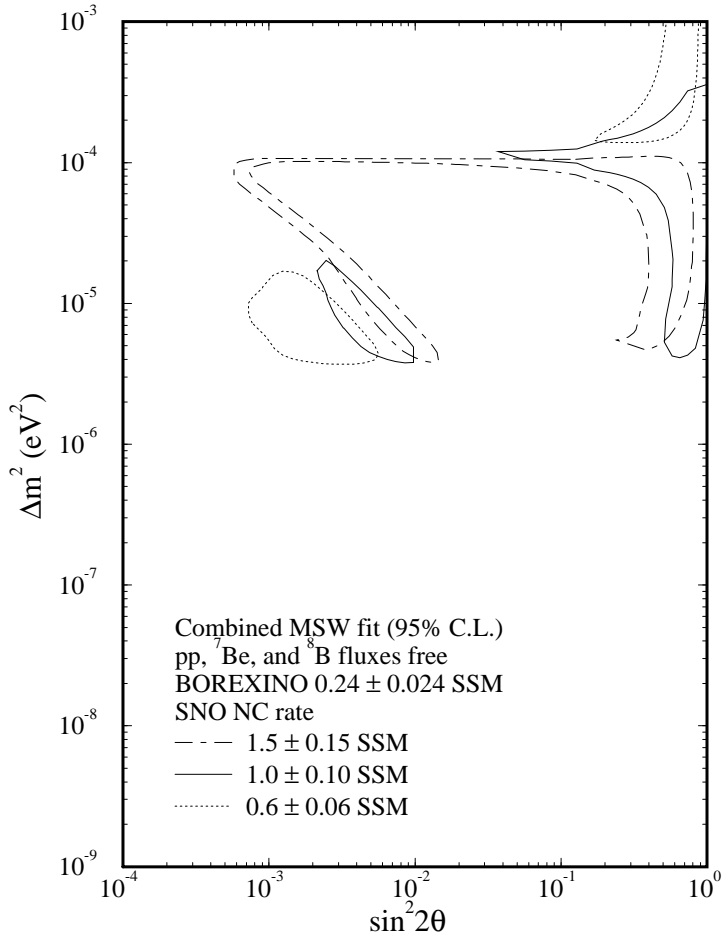


(a) Different SNO NC values

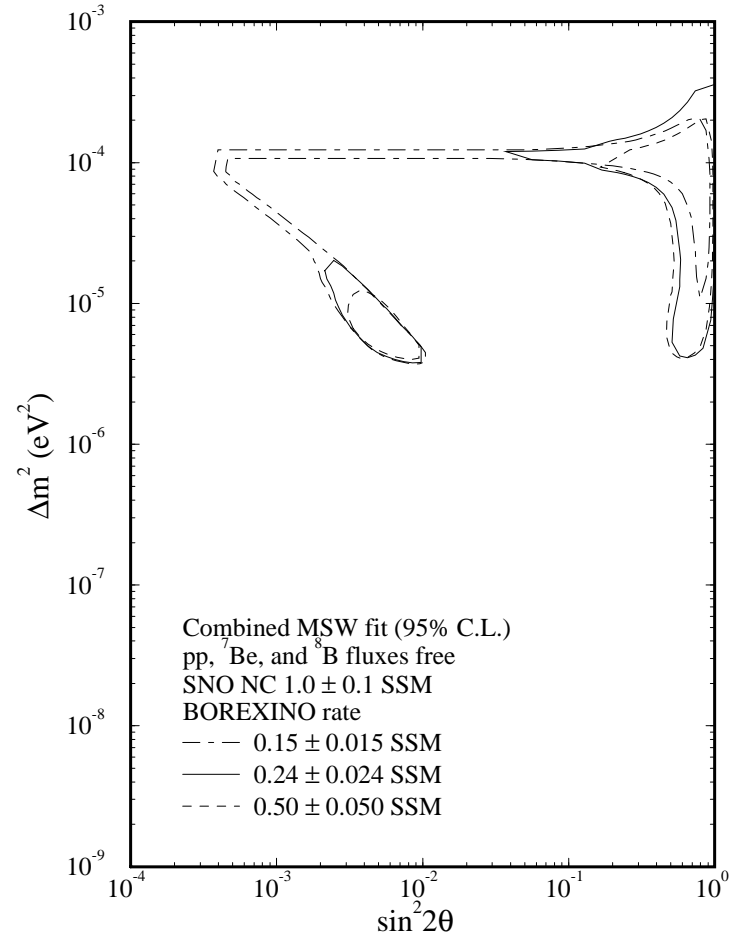


(b) Different BOREXINO values

FIG. 16. The flux constraints when the combined existing data plus possible results from both SNO and BOREXINO are considered. The projected experimental results are motivated by the MSW small-angle (nonadiabatic) solution. The constraints are for (a) different SNO NC rates and (b) different BOREXINO rates. These are 5 parameter fits (2 MSW parameters and 3 fluxes) to 5 data points (3 existing data plus 2 future results) with the luminosity constraint.

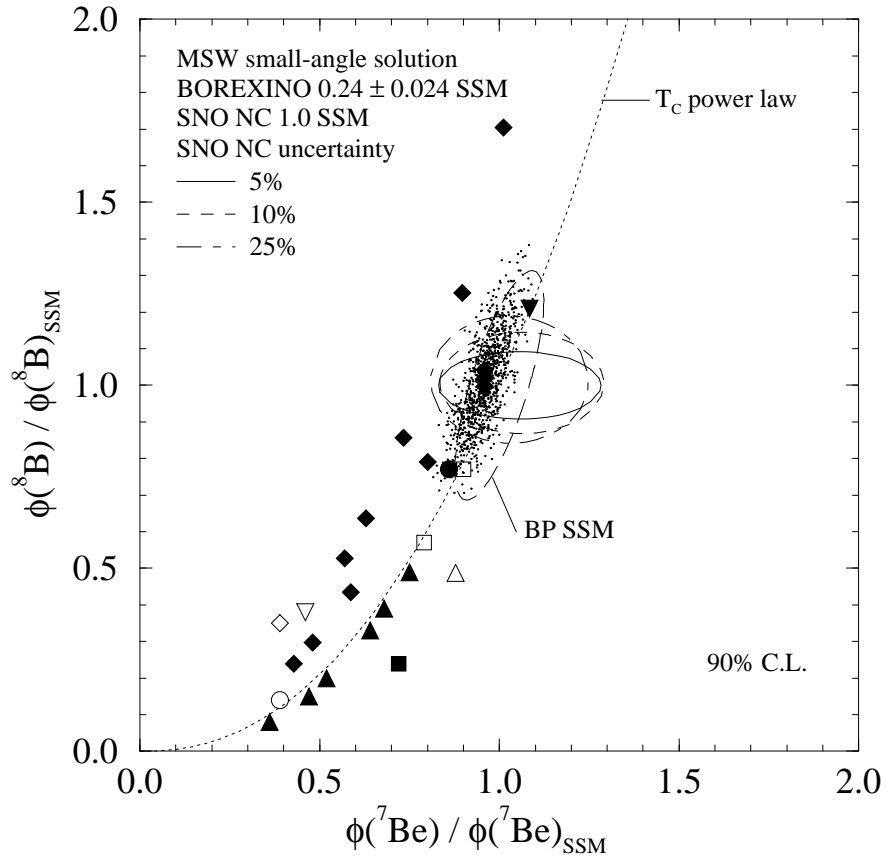


(a) Different SNO NC rates

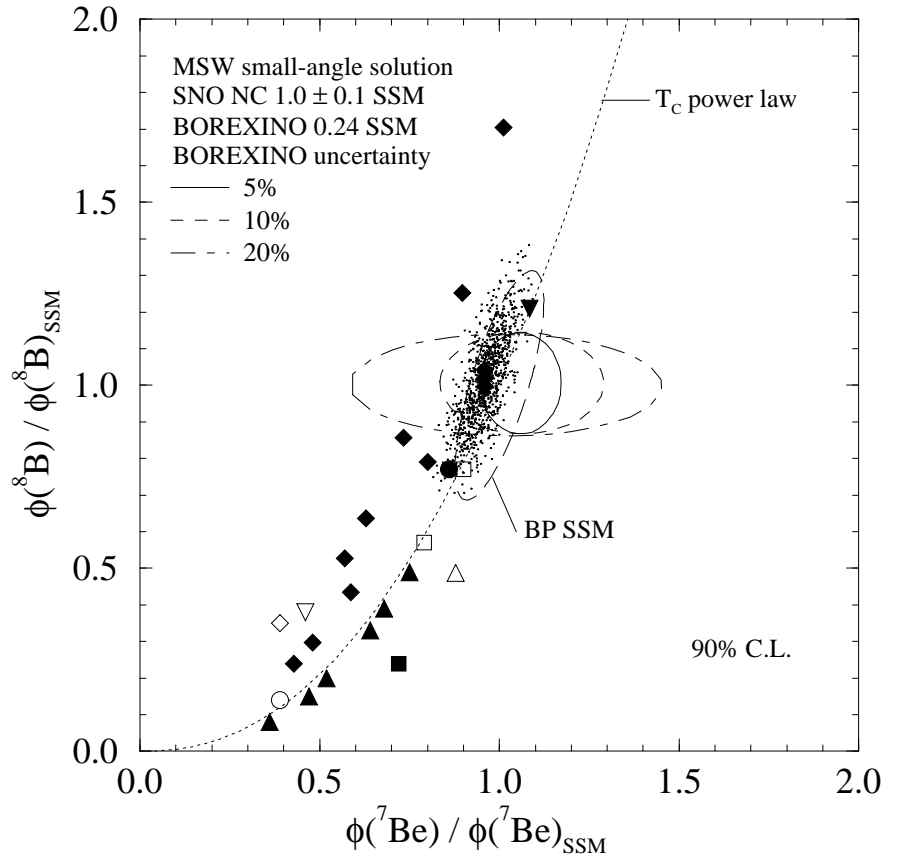


(b) Different BOREXINO rates

FIG. 17. The MSW allowed region when the  $pp$ ,  ${}^7\text{Be}$ , and  ${}^8\text{B}$  fluxes are fit as free parameters with the luminosity constraint. The existing data plus the results from SNO NC and BOREXINO are used. We assume (a) different SNO NC rates with a fixed BOREXINO rate and (b) different BOREXINO rates with a fixed SNO NC rate. The constraints for the fluxes with similar assumptions are shown in Fig. 16 and 22. Using the CNO flux as an additional free parameter does not change the allowed regions significantly.



(a) Sensitivity for SNO NC uncertainty



(b) Sensitivity for BOREXINO uncertainty

FIG. 18. The flux constraints for the MSW nonadiabatic region for various measurement uncertainties in (a) SNO and (b) BOREXINO. The existing data are also included in the fits.

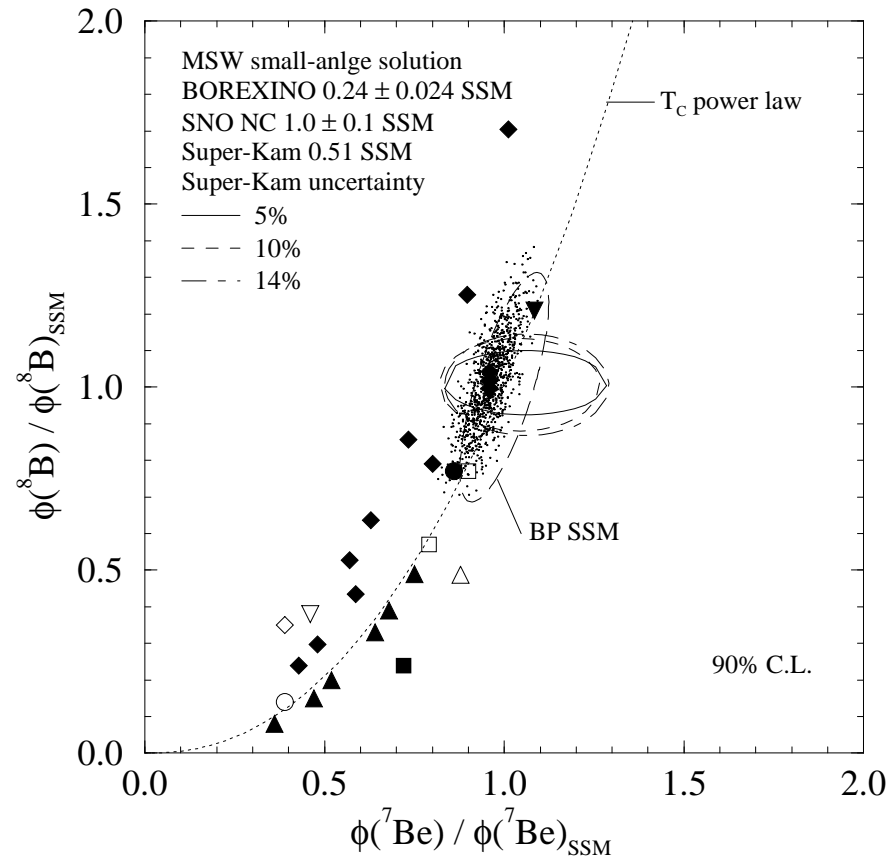


FIG. 19. The flux constraint when hypothetical Super-Kamiokande results for various measurement uncertainties are included. The joint fit also includes the existing data and the hypothetical SNO NC and BOREXINO results. The MSW parameters are in the nonadiabatic region.

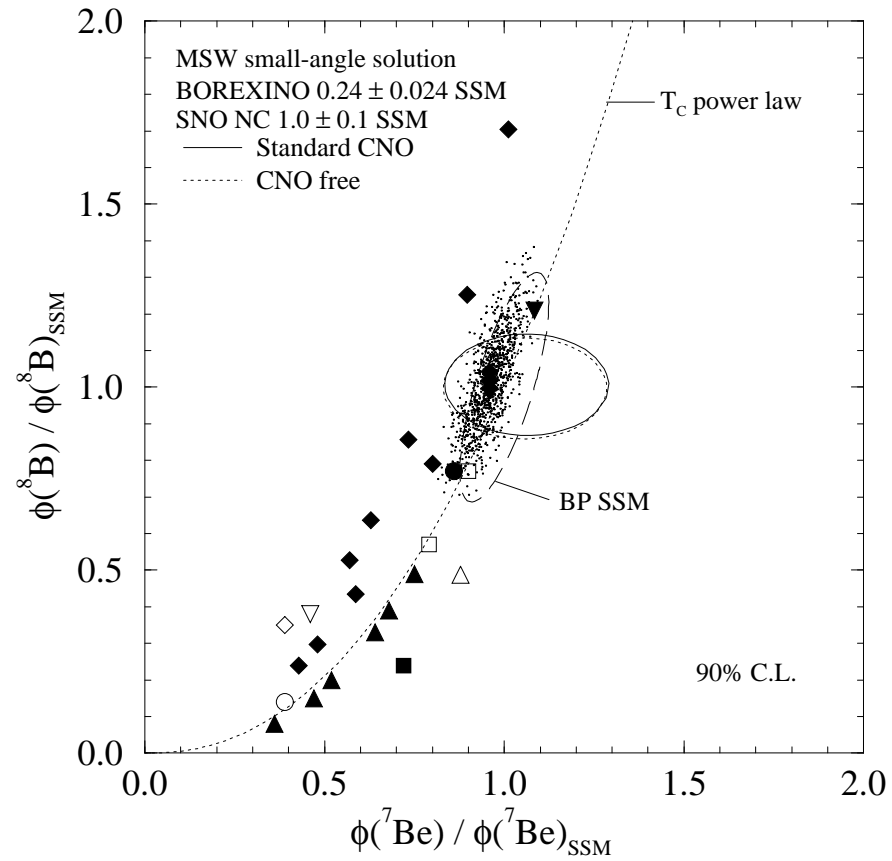
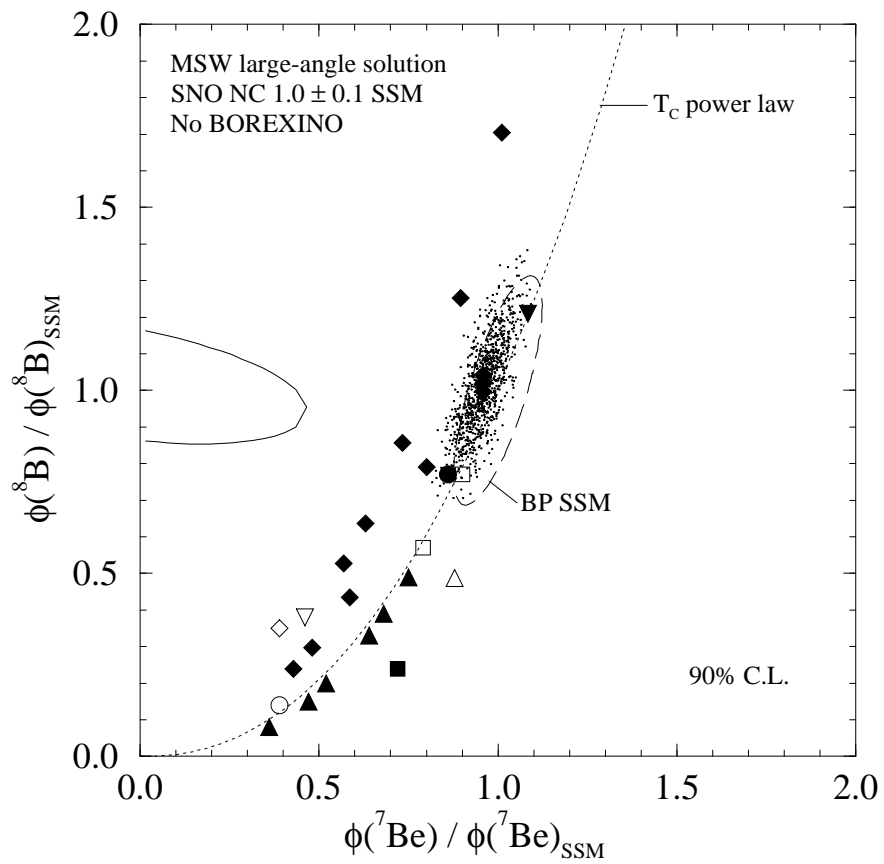
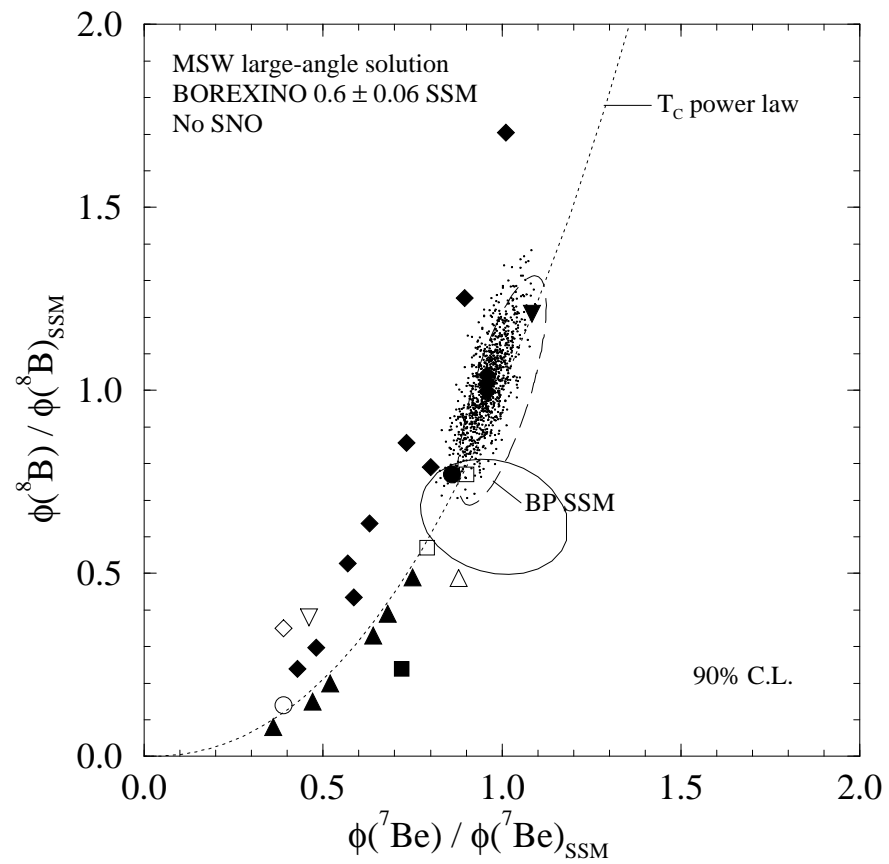


FIG. 20. The flux constraints when the CNO flux is used as an additional free parameter. The joint fit includes the existing data and the hypothetical SNO NC and BOREXINO results. The MSW parameters are in the nonadiabatic region.



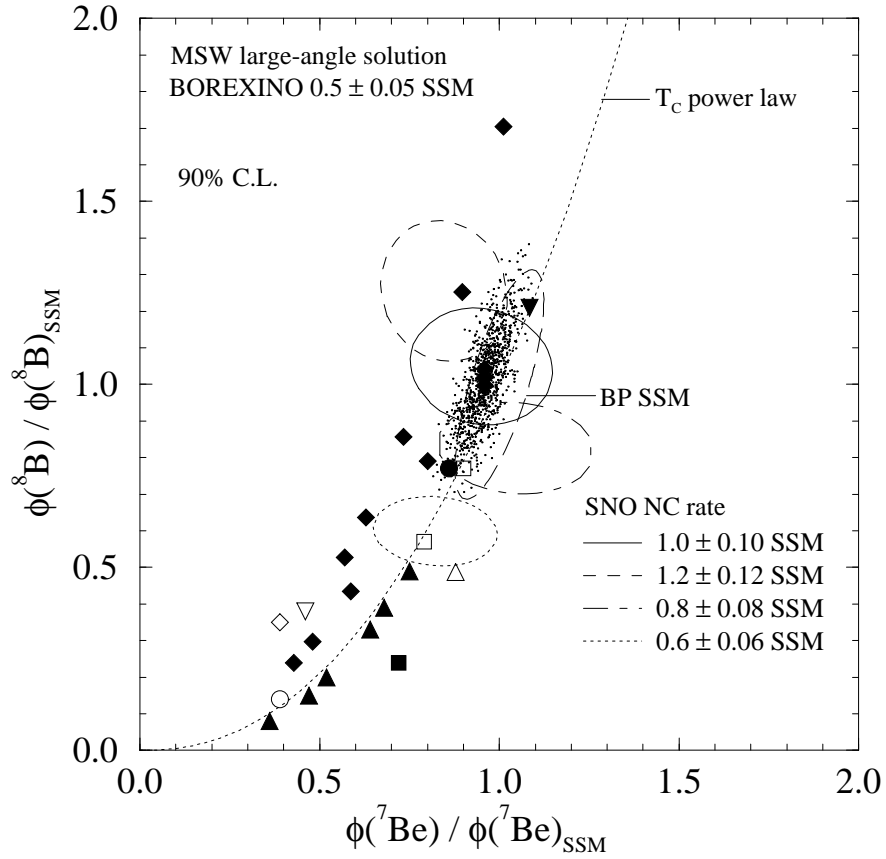
(a) SNO NC



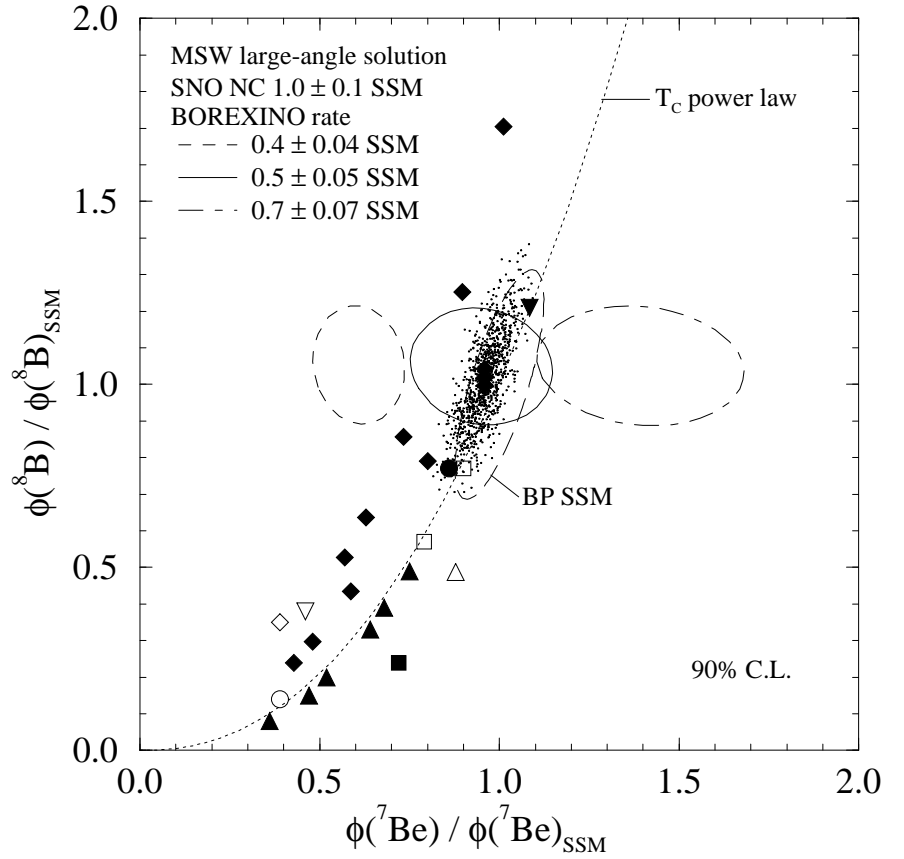
(b) BOREXINO

FIG. 21. Same as Fig. 15, but the MSW parameters are in the large-angle region.





(a) Different SNO NC values



(b) Different BOREXINO values

FIG. 22. Same as Fig. 16, but the MSW parameters are in the large-angle region.

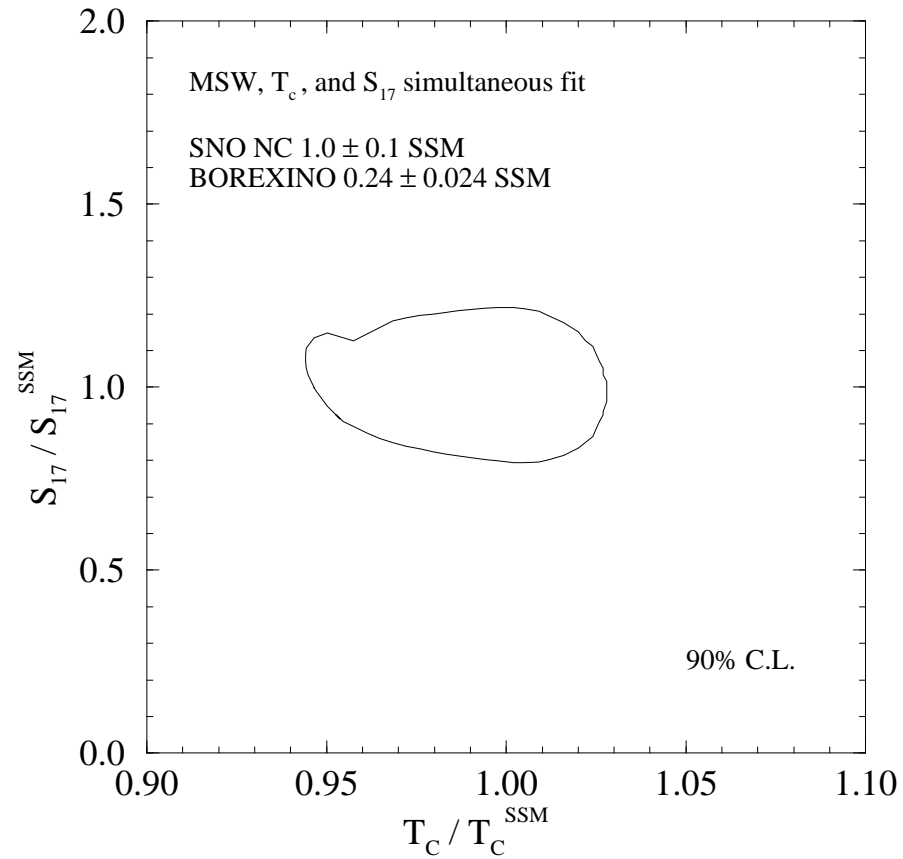


FIG. 23. The constraints for  $T_C$  and  $S_{17}$  in the presence of MSW oscillations when the existing data plus both hypothetical SNO NC and BOREXINO results are considered. This is a 4 parameter fit (2 MSW parameters plus  $T_C$  and  $S_{17}$ ) to 5 data points (3 existing data plus 2 hypothetical results) with the luminosity constraint.